Disruption of amyloid precursor protein ubiquitination selectively increases amyloid β (Aβ) 40 levels via presenilin 2-mediated cleavage

Received for publication, September 17, 2017, and in revised form, September 30, 2017 Published, Papers in Press, October 11, 2017, DOI 10.1074/jbc.M117.818138

Rebecca L. Williamson[‡], Karine Laulagnier[§1,2], André M. Miranda[‡¶‖3], Marty A. Fernandez[**], Michael S. Wolfe[4], Rémy Sadoul[§2], and Gilbert Di Paolo[‡‡‡5]**

*From the [‡]Department of Pathology and Cell Biology and the [‡‡]Taub Institute for Research on Alzheimer's Disease and the Aging Brain, Columbia University Medical Center, New York, New York 10032, the [§]Grenoble Institut des Neurosciences, Inserm, Grenoble 38042, France, the [¶]Life and Health Sciences Research Institute, School of Medicine, University of Minho and [‖]Life and Health Sciences Research Institute/3B's Research Group–Biomaterials, Biodegradables, and Biomimetics Associate Laboratory, 4710-057 Braga/Guimarães, Portugal, and the **Center for Neurologic Diseases, Harvard University, Boston, Massachusetts 02115*

Edited by Paul E. Fraser

Amyloid plaques, a neuropathological hallmark of Alzheimer's disease, are largely composed of amyloid β (Aβ) peptide, derived from cleavage of amyloid precursor protein (APP) by β- and γ-secretases. The endosome is increasingly recognized as an important crossroad for APP and these secretases, with major implications for APP processing and amyloidogenesis. Among various post-translational modifications affecting APP accumulation, ubiquitination of cytodomain lysines may represent a key signal controlling APP endosomal sorting. Here, we show that substitution of APP C-terminal lysines with arginine disrupts APP ubiquitination and that an increase in the number of substituted lysines tends to increase APP metabolism. An APP mutant lacking all C-terminal lysines underwent the most pronounced increase in processing, leading to accumulation of both secreted and intracellular Aβ40. Artificial APP ubiquitination with rapalog-mediated proximity inducers reduced Aβ40 generation. A lack of APP C-terminal lysines caused APP redistribution from endosomal intraluminal vesicles (ILVs) to the endosomal limiting membrane, with a subsequent decrease in APP C-terminal fragment (CTF) content in secreted exosomes, but had minimal effects on APP lysosomal degradation. Both the increases in secreted and intracellular Aβ40 were abolished by depletion of presenilin 2 (PSEN2), recently shown to be enriched on the endosomal limiting membrane compared with PSEN1. Our findings demonstrate that ubiquitin can act as a signal at five cytodomain-located lysines for endosomal sorting of APP. They further suggest that disruption of APP endosomal sorting reduces its sequestration in ILVs and results in PSEN2-mediated processing of a larger pool of APP-CTF on the endosomal membrane.

Alzheimer's disease (AD)[6] is the most common cause of late life dementia and is characterized clinically by a progressive decline in cognitive function and neuropathologically by the presence of extracellular amyloid plaques and intracellular neurofibrillary tangles (1). The main component of amyloid plaques is aggregated amyloid β (Aβ), a 4-kDa peptide formed by sequential cleavage of amyloid precursor protein (APP) by β- and γ-secretases (1). Like many other type 1 transmembrane proteins, APP is initially transported to the plasma membrane via biosynthetic and secretory pathways, where it is processed primarily by α-secretase in the non-amyloidogenic pathway (1–3). Alternatively, APP is rapidly endocytosed in a clathrin-dependent manner and delivered to endosomes, where amyloidogenic processing by β-site amyloid precursor protein cleaving enzyme 1 (BACE1) largely occurs, releasing the soluble ectodomain of APP (sAPPβ) luminally and the membrane-bound C-terminal fragment β (CTFβ) (2, 4–8). BACE1 is concentrated on endosomes and is highly active in the acidic environment of these organelles (9–13). After BACE1 processing, the CTFβ fragment is cleaved within the transmembrane domain by γ-secretase, releasing Aβ and APP intracellular domain (AICD). γ-Secretase cleaves C99 in a sequential fashion, releasing multiple Aβ peptides of different lengths (14). Of these, the most abundant is Aβ40, although longer peptides, such as Aβ42, are more prone to aggregation and generally

This work was supported in part by National Institutes of Health Grants R01 NS056049 (to G. D. P. and Ronald Liem), F30 AG047748 (to R. L. W.), and AG015379 (to M. S. W. and Dennis J. Selkoe). G. D. P. is a full time employee of Denali Therapeutics Inc. The content is solely the responsibility of the authors and does not necessarily represent the official views of the National Institutes of Health.

This article contains supplemental Fig. S1.

[1] Supported by the Fondation Plan Alzheimer.

[2] Supported by Inserm, Université Grenoble Alpes, France Alzheimer Foundation.

[3] Supported by Fundação para a Ciência e Tecnologia Grant PD/BD/105915/2014.

[4] Present address: Dept. of Medicinal Chemistry, University of Kansas, Lawrence, KS 66045.

[5] To whom correspondence should be addressed: Dept. of Pathology and Cell Biology, Columbia University Medical Center, 630 West 168th St., P&S 12-510, New York, NY 10032. E-mail: gd2175@cumc.columbia.edu.

[6] The abbreviations used are: AD, Alzheimer's disease; APP, amyloid precursor protein; Aβ, amyloid β; ILV, intraluminal vesicle; CTF, C-terminal fragment; FAD, familial AD; LOAD, late-onset AD; ANOVA, analysis of variance; AICD, APP intracellular domain; ESCRT, endosomal sorting complex required for transport; BisTris, 2-[bis(2-hydroxyethyl)amino]-2-(hydroxymethyl) propane-1,3-diol; Tricine, *N*-[2-hydroxy-1,1-bis(hydroxymethyl)ethyl] glycine; CHAPSO, 3-[(3-cholamidopropyl)dimethylammonio]-2-hydroxy-1-propanesulfonic acid; DIV, days *in vitro*; MVE, multivesicular endosome; ERAD, endoplasmic reticulum-associated degradation; GWAS, genome-wide association study; PI3P. phosphatidylinositol 3-phosphate; CHX, cycloheximide; sAPP, soluble APP; FL-APP, full-length APP.

more synapto- and neurotoxic (1). In familial AD (FAD), overall levels of Aβ increase, or there is a shift in Aβ production that increases the ratio of Aβ42/40. However, in the majority of AD cases, which occur sporadically as late-onset AD (LOAD), mechanisms of Aβ accumulation remain poorly understood, although they likely also involve reduced Aβ clearance (15).

It is now well-established that endosomes represent a key intracellular station for APP processing and that endosomal dysfunction is a pathophysiological hallmark of AD (16–18). Several susceptibility genes associated with LOAD from genome-wide association studies (GWAS) are endosomal regulators (19–22), and specific defects in endosomal sorting pathway components have been associated with LOAD (8, 23). For example, the retromer pathway, which traffics protein cargo from the endosome to the *trans*-Golgi network or the cell surface, has been implicated in APP trafficking and processing and is found deficient in vulnerable brain regions from patients with LOAD (24–27). APP and its proteolytic enzymes are transmembrane proteins that traffic through the secretory pathway and endolysosomal system, and thus the sorting and compartmentalization of these proteins dictates processing of APP into Aβ and other fragments.

In normal neuronal metabolism, Aβ is produced and secreted from the cell at low levels. However, intraneuronal increases in Aβ are toxic and precede the gross pathological changes of AD (28, 29). AD-affected neurons accumulate Aβ, particularly in multivesicular endosomes (MVEs) (30, 31), which consist of a limiting membrane containing intraluminal vesicles (ILVs). The endosomal sorting complex required for transport (ESCRT) is a series of protein complexes (ESCRT-0 to ESCRT-III) that form ILVs by invagination of the MVE limiting membrane, sequestering specific protein cargo inside. Several studies implicate APP as a protein cargo that can be recognized and sorted by ESCRT (7, 32, 33). In ILVs, cargo can undergo several fates, including lysosomal degradation and extracellular secretion as exosomes. Underscoring the pathophysiological significance of ILV sorting for APP, silencing of CD2-associated protein (CD2AP), an endosomal regulator associated with increased risk for LOAD, has recently been shown to lead to an increase in intracellular Aβ42 in neuronal dendrites by interfering with sorting of APP from the endosomal limiting membrane to the ILVs and thereby preventing APP degradation in lysosomes (34).

Sorting of transmembrane proteins can be controlled by ubiquitination, a post-translational modification that can signal multiple fates, including proteasomal degradation, endoplasmic reticulum-associated degradation (ERAD), endocytosis, or sorting in the MVE via ESCRT (35). Ubiquitin is a 76-amino acid peptide that is covalently attached to lysine residues of a protein cargo via sequential enzymatic reactions of E1, E2 and E3 ubiquitin ligases (35). The E3 ubiquitin ligase(s) specific for APP remains uncertain, but some studies suggest promising candidates (36, 37), and a recent GWAS of Caribbean Hispanics identified F-box/leucine rich-repeat protein 7 (FBXL7), a subunit of an E3 ligase, to be associated with LOAD (38). Several reports identify ubiquitination sites on APP (37, 39, 40) or report alterations in Aβ levels due to changes in APP ubiquitination (7, 36, 41), but they do not investigate in depth of the mechanism underlying this phenomenon or the downstream effects of reduced ubiquitination. APP contains five C-terminal lysines that could potentially be ubiquitinated: Lys-724, Lys-725, Lys-726, Lys-751, and Lys-763. Two studies identified APP in screens of the ubiquitome. Kim *et al.* (39) showed ubiquitination of APP Lys-751 and Lys-763 in a screen of HCT116 cells after proteasomal inhibition and affinity purification using an antibody that recognizes the di-glycine remnant of ubiquitinated proteins. Similarly, Wagner *et al.* (40) identified ubiquitination of APP Lys-751 and Lys-763 in a screen of the ubiquitome in unperturbed HEK-293T cells. Several studies have looked specifically at APP ubiquitination. Watanabe *et al.* (36) showed that FBL2 induces APP ubiquitination at Lys-726, leading to a reduction in Aβ generation, attributed to increased APP proteasomal degradation. El Ayadi *et al.* (41) showed that ubiquilin-1 induces APP ubiquitination at Lys-763 to sequester APP in the Golgi and prevent maturation. Bustamante *et al.* (42) showed that expression of C99, with all five C-terminal lysines substituted to arginine, is not degraded as efficiently as wild-type C99 and accumulates in Golgi-like structures, potentially due to a deficiency in ERAD. In a screen of interactors for the APP cytodomain, Del Prete *et al.* (37) identified a number of components of ubiquitin-processing machinery, including several E3 ubiquitin ligases and deubiquitinases, and showed that all five C-terminal lysines were ubiquitinated in mouse brain). Thus, it appears that all five C-terminal lysines may be ubiquitinated physiologically.

We have previously identified a string of lysine residues in the juxtamembrane region of APP, mutation of which led to a redistribution of APP from ILVs to the limiting membrane and a subsequent alteration of APP processing (7). However, the terminal two APP lysines in the cytodomain were still capable of ubiquitination in that analysis; thus, it did not fully represent a model of lack of APP ubiquitination. Here, we show that loss of APP ubiquitination achieved by systematic substitution of all the cytodomain lysines residues has a profound impact on APP endosomal trafficking and metabolism. Specifically, we found that decreased ubiquitination causes defects in APP sorting into ILVs and exosomal release of APP-CTFs as well as an increase in Aβ production by PSEN2-containing γ-secretase complex, which is localized to the endosomal limiting membrane (43). The increase is specific to Aβ40, thus decreasing the Aβ42/40 ratio in a manner known to be protective against Aβ aggregation and toxicity (44, 45). Our data thus underscore the importance of ubiquitination as a signal for endosomal sorting of APP and contribute to growing recognition of γ-secretase composition as a significant factor in differential APP processing.

Results

APP lysine mutations lead to a deficiency in ubiquitination

To assess whether the five lysines present in the APP C-terminal domain (Fig. 1*A*) are sites of ubiquitination, we generated a panel of GFP-tagged APP mutants with each lysine mutated to arginine individually and in several combinations. We have previously shown that mutation of three consecutive lysines in the

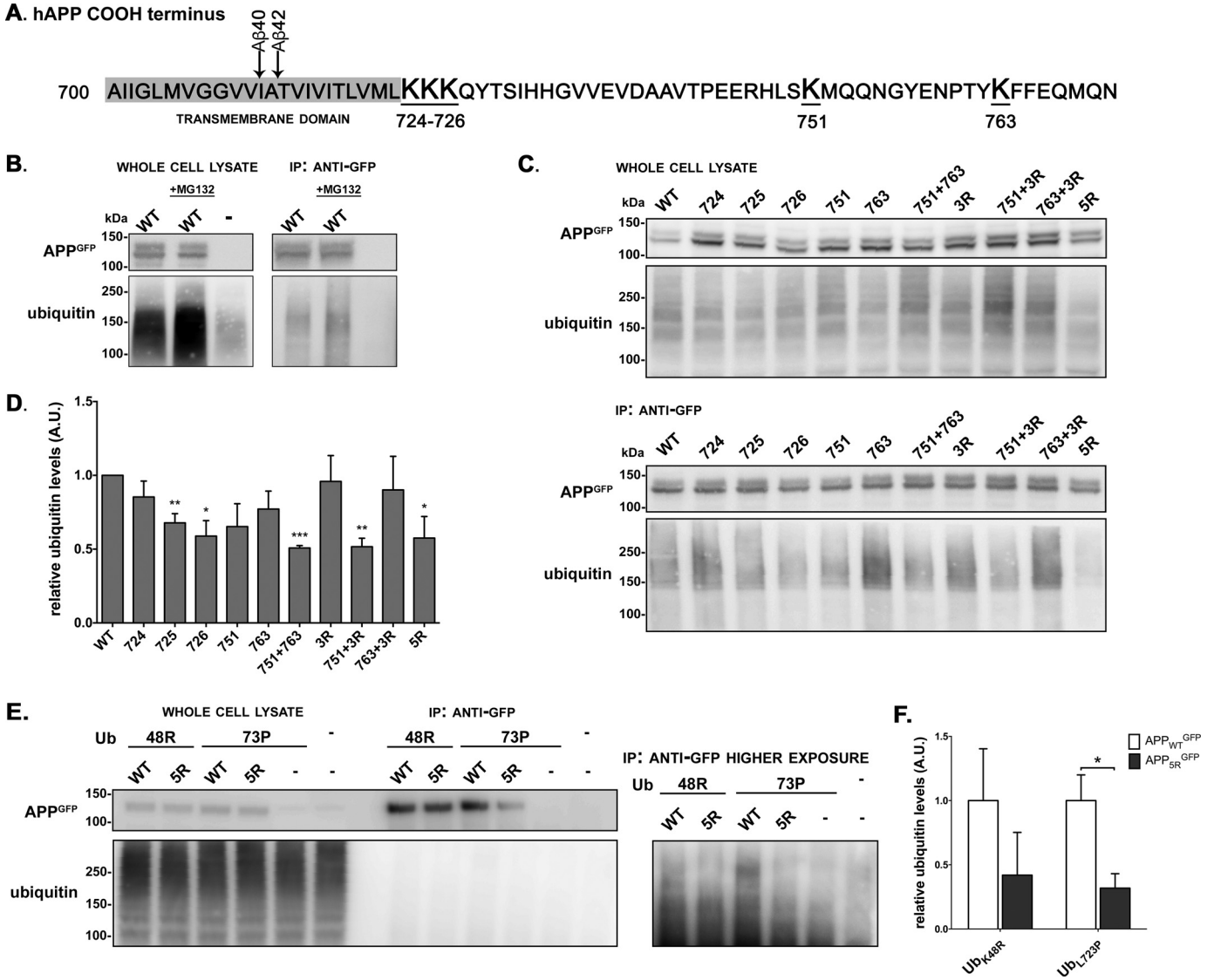

Figure 1. Mutation of APP-770 C-terminal lysines leads to a deficiency in APP ubiquitination. *A,* hAPP C-terminal domain contains 5 lysine residues that are potential sites of ubiquitination. Aβ40 and Aβ42 *arrows* indicate sites of γ-secretase cleavage. *B,* representative Western blot of APP ubiquitin immunoprecipitation (*IP*) in HEK-293T cells with co-expression of Ub^{HA} and $APP_{WT}{}^{GFP}$ and untransfected (indicated by $-$), untreated, or after 4 h of treatment with 20 μM MG-132. *C,* representative Western blot of APP ubiquitin immunoprecipitation in HEK-293T cells with co-expression of $Ub_{K48R}{}^{HA}$ and APP^{GFP} lysine-to-arginine mutant. *Numbered lanes* indicate APP lysine residue(s) mutated to arginine (WT = wild type; 3R = APP K724R/K725R/K726R; 5R = all C-terminal lysines mutated). *D,* quantification of immunoprecipitated ubiquitin levels, normalized to immunoprecipitated APP^{GFP} and expressed in arbitrary units (*A.U.*) relative to $APP_{WT}{}^{GFP}$. Values denote mean $\pm$ S.E., $n = 4$ biological replicates. *, $p < 0.05$; **, $p < 0.01$; ***, $p < 0.001$ as measured by one-tailed, one sample Student's *t* test. The one-tailed test was used based on the prediction that mutating lysines would cause decreased ubiquitination. *E,* Western blot of APP ubiquitin (*Ub*) IP in N2a cells co-expressing $APP_{WT}{}^{GFP}$ or $APP_{5R}{}^{GFP}$ and $Ub_{K48R}{}^{HA}$ or $Ub_{L73P}{}^{mCherry}$, immunoprecipitated by anti-GFP. *Lanes* indicate both ubiquitin mutation (*Ub*) and APP^{GFP} mutation. *Right panel* shows higher exposure of same anti-ubiquitin Western blotting. *F,* quantification of immunoprecipitated ubiquitin levels, with immunoprecipitated $APP_{5R}{}^{GFP}$ normalized to immunoprecipitated $APP_{WT}{}^{GFP}$ in each case and expressed in arbitrary units (*A.U.*) relative to $APP_{WT}{}^{GFP}$. Values denote mean $\pm$ S.E., $n = 3$ biological replicates. *, $p < 0.05$ as measured by Student's *t* test.

juxtamembrane region, Lys-724 – Lys-726, to arginine (termed APP_{3R}) leads to a deficiency of ubiquitination of exogenously expressed APP by endogenous ubiquitin in HeLa cells (7). APP constructs with individual mutations K724R, K725R, and K726R allow us to identify whether all three of these residues are necessary for APP ubiquitination. Two downstream residues, Lys-751 and Lys-763, which have been identified as sites of ubiquitination in several screens (37, 39, 40), suggest that the APP_{3R} mutant may have residual ubiquitination at these two lysines. We thus generated APP mutant constructs with several combinations of lysine-to-arginine mutations, including five individual lysine mutations, the previously studied APP_{3R} mutant (K724R/K725R/K726R) as well as APP K751R + K763R, APP K724R/K725R/K726R + K751R, APP K724R/K725R/K726R + K763R, and mutation of all five lysines, termed APP_{5R}.

Polyubiquitination occurs when ubiquitin chains assemble at any of seven lysine residues of ubiquitin and can signal different fates for the targeted protein. The UbK48 chain directs protein cargo to the proteasome for degradation (46). To hinder this pathway, we co-expressed APP^{GFP} constructs in cells with $Ub_{K48R}{}^{HA}$, a ubiquitin mutant which cannot form UbK48 polyubiquitin chains. Indeed, we are specifically interested in ubiquitination of APP as a signal for membrane trafficking, and

this allows us to study those polyubiquitin signals more likely to be involved in trafficking, such as UbK63 polyubiquitination or monoubiquitination (35). As a control, we show that the ubiquitin signal in the anti-GFP immunoprecipitate of HEK-293T cells co-transfected with APP^{GFP} and Ub^{HA} is a smear above ~130 kDa, suggesting multi- or polyubiquitination of $APP_{WT}{}^{GFP}$ (Fig. 1*B*). Pre-treatment with 20 μM MG-132, a proteasome inhibitor, did not alter the levels of full-length APP (FL-APP) nor did it increase the polyubiquitin smear in the immunoprecipitate, indicating that ubiquitinated APP^{GFP} is not degraded by the proteasome. To measure the level of ubiquitination of the APP^{GFP} lysine-to-arginine mutants, we co-expressed each in HEK-293T cells with $Ub_{K48R}{}^{HA}$, then immunoprecipitated the exogenous APP^{GFP} with an anti-GFP antibody, and quantified the level of ubiquitin via Western blotting (Fig. 1, *C* and *D*). Several APP mutants showed a decrease in ubiquitination as compared with $APP_{WT}{}^{GFP}$, indicating that most APP C-terminal lysine residues can be ubiquitinated or that there is a level of redundancy between the residues. Of note, K751R + K763R and APP_{3R} + K751R had consistently lower levels of ubiquitination, indicating that the Lys-751 residue may be an important residue. Although the $APP_{5R}{}^{GFP}$ mutant lacks all C-terminal lysines and thus should not be ubiquitinated, there was some residual ubiquitin signal in the APP^{GFP} immunoprecipitation, which may be attributed to aberrant ubiquitination of N-terminal lysines or ubiquitination of APP^{GFP}-interacting partners that co-immunoprecipitate. Untagged APP_{5R} immunoprecipitated with an anti-APP antibody still exhibited residual ubiquitin signal, suggesting that it is not due to ubiquitination of the GFP tag (data not shown). We had previously shown a deficiency in ubiquitination of $APP_{3R}{}^{GFP}$ (7) in studying endogenous ubiquitination of APP in HeLa cells. However, we did not see a similar deficiency in HEK-293T cells co-expressing $APP_{3R}{}^{GFP}$ and $Ub_{K48R}{}^{HA}$ (Fig. 1*D*), possibly indicating differences in cell types or in the ubiquitin chain linkages modifying the two downstream APP lysines. This discrepancy underlines the importance of studying the $APP_{5R}{}^{GFP}$ mutant to understand the effect of complete lack of APP cytodomain ubiquitination.

For the remainder of the experiments, N2a cells were used instead of HEK-293T cells because 1) they are of neural origin, 2) they release detectable amounts of Aβ42, and 3) their mouse origin allows us to distinguish exogenous human APP^{GFP} fragments from endogenous murine APP. In N2a cells, the ubiquitination of APP^{GFP} was more difficult to detect, even with co-transfection of $Ub_{K48R}{}^{HA}$, rendering it more difficult to quantify ubiquitination of all APP mutants in this cell line. We reasoned that this could be due to a shorter half-life of ubiquitinated species of APP^{GFP} in this cell line, and we chose to confirm the decrease in ubiquitination of the $APP_{5R}{}^{GFP}$ mutant in N2a cells in a model of stabilized ubiquitination. By co-expressing APP^{GFP} in N2a cells with $Ub_{L73P}{}^{mCherry}$, a ubiquitin mutant that is resistant to deubiquitinases (47), we were able to detect an accumulation of ubiquitinated $APP_{WT}{}^{GFP}$, as compared with cells expressing $Ub_{K48R}{}^{HA}$. With expression of $Ub_{L73P}{}^{mCherry}$, we could detect a significant reduction in levels of ubiquitination of $APP_{5R}{}^{GFP}$ compared with $APP_{WT}{}^{GFP}$; however, there was only a trend toward significance in the N2a cells co-transfected with $Ub_{K48R}{}^{HA}$ perhaps in part due to the lower signal-to-noise ratio (Fig. 1, *E* and *F*). This indicates that $APP_{5R}{}^{GFP}$ undergoes less ubiquitination than $APP_{WT}{}^{GFP}$, as predicted. Accumulation of ubiquitinated APP with co-expression of $Ub_{L73P}{}^{mCherry}$ is consistent with the existence of a pool of transiently ubiquitinated APP that leads to a short-lived ubiquitination signal. Although the transient nature of this ubiquitin signal makes it difficult to detect (as also suggested by our failed attempts to profile the ubiquitination sites of APP by mass spectrometry), it may represent an important regulator of APP trafficking and processing.

Lysine-to-arginine APP mutants are highly metabolized

We next investigated the effect of ubiquitin deficiency on the metabolism of APP in cultured cells. We expressed APP^{GFP} lysine-to-arginine mutants in N2a cells, and we measured the fragments that are produced by cleavage of FL-APP^{GFP} by Western blotting or ELISA (Fig. 2*A*). When expressed in N2a cells, all APP^{GFP} lysine-to-arginine mutants exhibited decreased amount of FL-APP^{GFP} (Fig. 2*B*). Consistent with increased processing of APP, we detected higher levels of the sAPPα and sAPPβ secreted into the culture media. There was a trend toward an increase in processing with the number of APP lysines mutated, such that the $APP_{5R}{}^{GFP}$ mutant, with no remaining lysines in the C-terminal domain, underwent the most extensive processing. Compared with $APP_{WT}{}^{GFP}$, the $APP_{5R}{}^{GFP}$ mutant had an approximate reduction of FL-APP^{GFP} of 50% and a corresponding 3-fold increase in cleaved soluble fragment sAPPα and 2-fold increase in cleaved soluble fragment sAPPβ, normalized to the expression levels of FL-APP^{GFP}. In line with increased processing, APP^{GFP} lysine-to-arginine mutants led to a selective increase in secreted Aβ40, with no change in Aβ42, thus causing a significant decrease in Aβ42/40 ratios in some APP mutants (Fig. 2*B*). Of note, there was high variability in the levels of Aβ42, likely because levels were closer to background, and the decrease in Aβ42/40 ratio was only evident in APP mutants with several lysines mutated.

We chose to focus further analysis on APP_{5R}, the mutant with the strongest phenotype in terms of APP processing, and because the APP_{3R} mutant has residual ubiquitination at the two C-terminal lysines. To confirm that the increase in Aβ40 generation of APP lysine-to-arginine mutants is due to deficiency of ubiquitination, we sought to determine whether artificial ubiquitination of the APP_{5R} mutant could reverse the phenotype. We generated constructs to express dimerizable APP and ubiquitin with DmrA and DmrC tags, respectively, based on a commercially available rapalog-induced dimerization system (48, 49). By expressing APP^{DmrA} and Ub^{DmrC} in N2a cells and adding A/C heterodimerizer, we can induce physical proximity between APP^{DmrA} and Ub^{DmrC} (Fig. 3*A*). Indeed, artificial ubiquitination of $APP_{5R}{}^{DmrA}$ reduced secretion of Aβ40 after treatment of heterodimerizer compared with control solution (ethanol) (Fig. 3*C*). Aβ42 levels were also decreased for both heterodimerizer-treated $APP_{WT}{}^{DmrA}$ and $APP_{5R}{}^{DmrA}$. The reduction in Aβ is not likely due to an increase in APP^{DmrA} degradation, because levels of FL-APP^{DmrA} are higher in heterodimerizer-treated cells as compared with control-treated cells (Fig. 3*D*). Of note, the cells expressing $APP_{5R}{}^{DmrA}$ alone

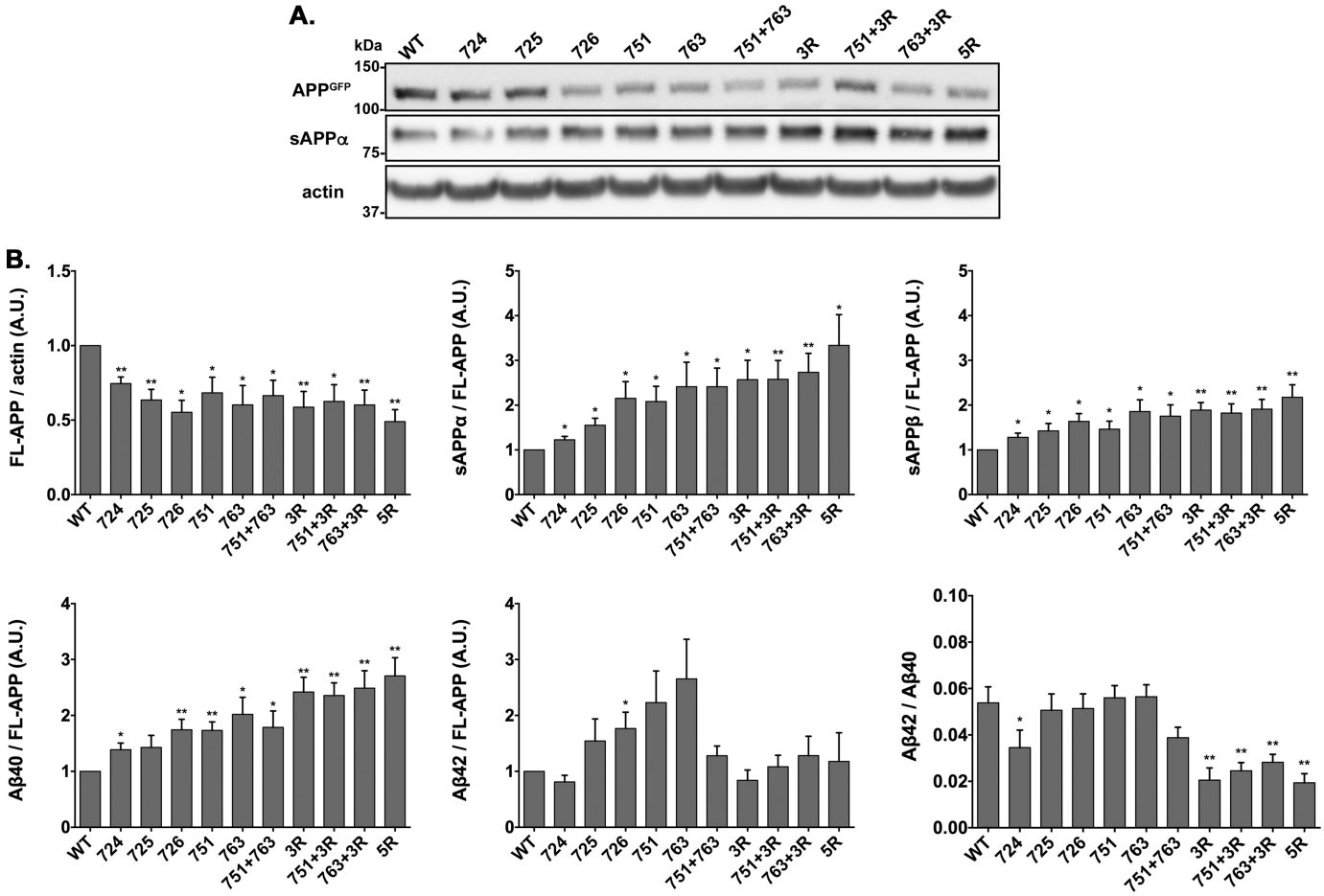

Figure 2. Metabolism of APP Lys → Arg mutants is altered in N2a cells. *A,* representative Western blot of full-length APP^{GFP} (FL-APP^{GFP}) and actin from cell lysate and sAPPα from cell media of N2a cells expressing APP^{GFP} lysine-to-arginine mutants. *Numbered lanes* indicate APP lysine residue(s) mutated to arginine (WT = wild type; 3R = APP K724R/K725R/K726R; 5R = all C-terminal lysines mutated). *B,* quantification of FL-APP^{GFP} and sAPPα (soluble N-terminal fragment from α-secretase cleavage) from Western blot, and quantification of Aβ40, Aβ42, and sAPPβ (soluble N-terminal fragment from β-secretase cleavage) by ELISA of cell culture media. FL-APP^{GFP} is normalized to actin loading control and sAPPα, sAPPβ, Aβ40, and Aβ42 are normalized to FL-APP^{GFP}. All are expressed in arbitrary units (*A.U.*) relative to APP$_{WT}^{GFP}$. Values denote mean ± S.E., n = 5–7 biological replicates. *, $p < 0.05$; **, $p < 0.01$, as measured by one sample Student's *t* test.

did not show a significant increase in Aβ40 compared with APP$_{WT}^{DmrA}$, which we speculate may be due to a shorter collection period of culture media (12 h compared with 24 h in all other experiments). This was necessary to preserve cellular viability in conditions containing the A/C heterodimerizer. We also note that the ethanol-treated cells had lower levels of FL-APP^{DmrA} compared with untreated and A/C heterodimerizer-treated conditions, which we do not have a clear explanation for but may be due to potential effects of ethanol on APP transcription, mRNA stability, or processing. In all, these results indicate that the chemically induced addition of ubiquitin to the C-terminal domain of APP mutants that are deficient in ubiquitination is sufficient to decrease levels of Aβ40, lending further support to the notion that the APP$_{5R}$-mediated increase in Aβ40 is due to a ubiquitin deficiency.

Importantly, we confirmed that the APP$_{5R}^{GFP}$ mutant is similarly processed in primary neuronal cultures, using lentivirus-mediated expression of APP^{GFP}, except levels of FL-APP^{GFP} were unchanged and levels of Aβ42 secreted by primary neurons were significantly decreased (Fig. 4, *A* and *B*). APP-CTF^{GFP} was not detectable in neuronal cultures under basal conditions; however, a band appears upon treatment with γ-secretase inhibitor, likely representing both CTFα and CTFβ. APP-CTF$_{5R}^{GFP}$ accumulates ~75% more than APP-CTF$_{WT}^{GFP}$ after γ-secretase inhibition, suggesting that γ-secretase cleaves more APP-CTF$_{5R}^{GFP}$ than APP-CTF$_{WT}^{GFP}$ (Fig. 4, *C* and *D*). Because ubiquitin can be a signal for endocytosis, the increase in sAPPα from both N2a cells and primary neuronal cultures expressing APP$_{5R}^{GFP}$ led us to hypothesize that APP$_{5R}^{GFP}$ was accumulating on the cell surface, where it is cleaved by α-secretase. However, in a biotinylation assay to quantify cell-surface levels of APP^{GFP}, we did not note any significant difference between surface levels of APP$_{WT}^{GFP}$ and APP$_{5R}^{GFP}$ normalized to total APP^{GFP} (Fig. 5*A*). We speculate that the increase in sAPPα may be due to an increase in cleavage of FL-APP^{GFP} that occurs on the endosomal membrane, because this is the predominant site of APP$_{5R}$ accumulation, or that α-secretase processing may occur in the secretory pathway before APP reaches the cell surface.

Because the APP lysine-to-arginine mutations include residues close to the γ-secretase cleavage site, we checked whether the increase in processing by γ-secretase could be due to a change in the interaction between γ-secretase and the APP mutant independently of potential differences in intracellular

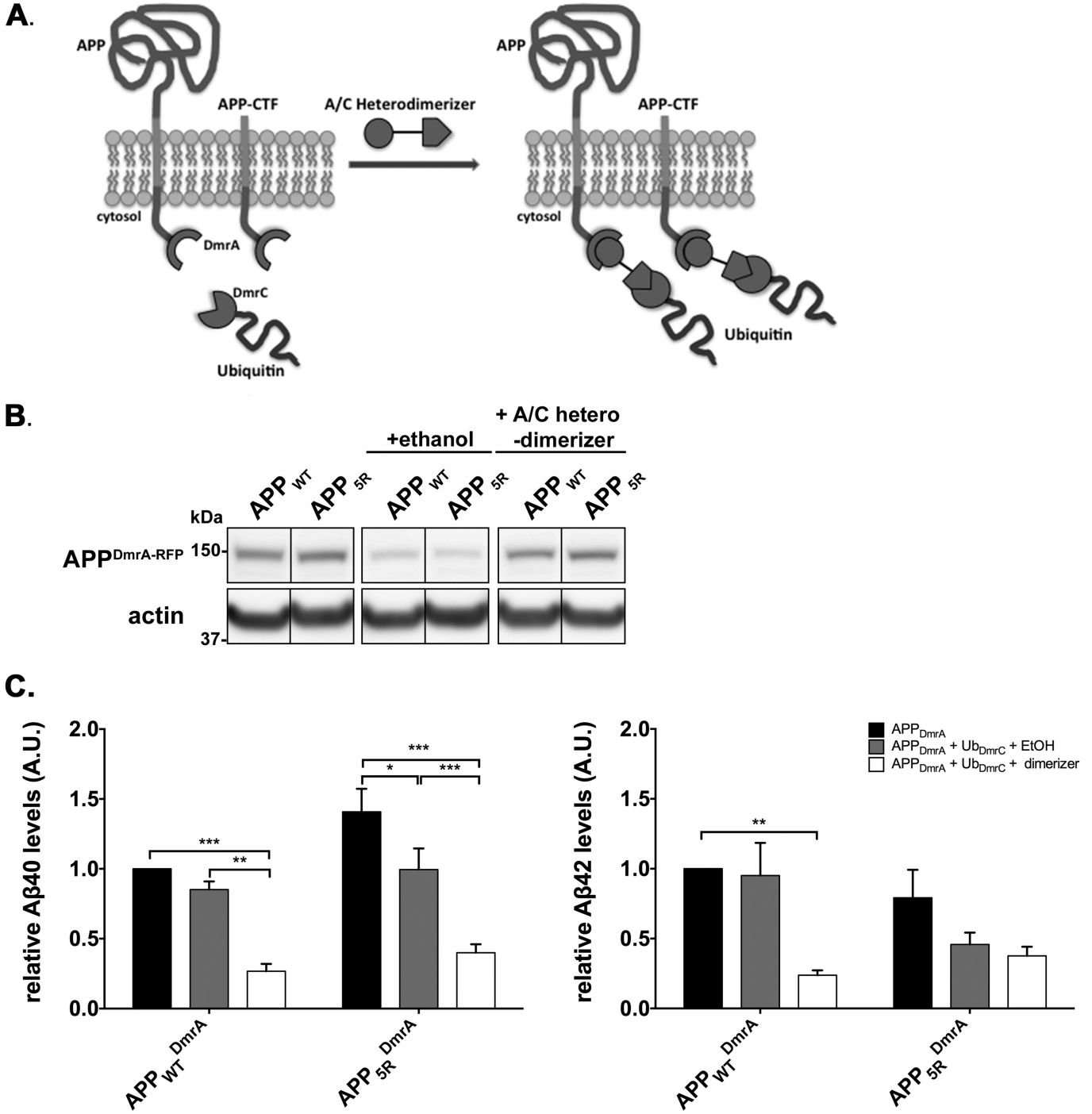

Figure 3. Chemically induced cross-linking of APP and ubiquitin decreases Aβ40 levels. *A,* diagram describing the dimerization of DmrA and DmrC domains fused to APP and ubiquitin, respectively, after addition of A/C heterodimerizer to culture media. *B,* representative Western blot of N2a cells expressing $APP^{DmrA\text{-}RFP}$ alone or co-expressing $APP^{DmrA\text{-}RFP}$ and Ub^{DmrC} were treated for 12 h with control solute ethanol or A/C heterodimerizer. *C,* cell culture media from *B* was measured for levels of secreted Aβ40 and Aβ42 measured via ELISA, and values are expressed in arbitrary units (*A.U.*) relative to $APP_{WT}^{DmrA\text{-}RFP}$ alone. Values denote mean ± S.E., $n = 3$–6 biological replicates. *, $p < 0.05$; **, $p < 0.01$; ***, $p < 0.001$ as measured by one sample Student's *t* test (between $APP_{WT}^{DmrA\text{-}RFP}$ and other samples) or regular Student's *t* test.

protein sorting. To this end, we generated and purified $C99^{WT}$ and $C99^{5R}$ and subjected them to cleavage by purified γ-secretase membranes in a cell-free assay, and we measured the levels of Aβ40 and Aβ42 produced (Fig. 5*B*). Using purified $C99^{5R}$ as a substrate did not result in any change in Aβ levels compared with $C99^{WT}$ (Fig. 5*B*). This suggests that the APP_{5R}-mediated increase in Aβ40 in cell culture is not simply due to an intrinsic change in the interaction of APP_{5R} with the γ-secretase complex, but it is more likely due to a change in APP trafficking, as hypothesized.

APP_{5R} is redistributed to endosomal limiting membrane

As membrane-bound cargo traffics through the endolysosomal system, it undergoes sorting at the endosomal mem-

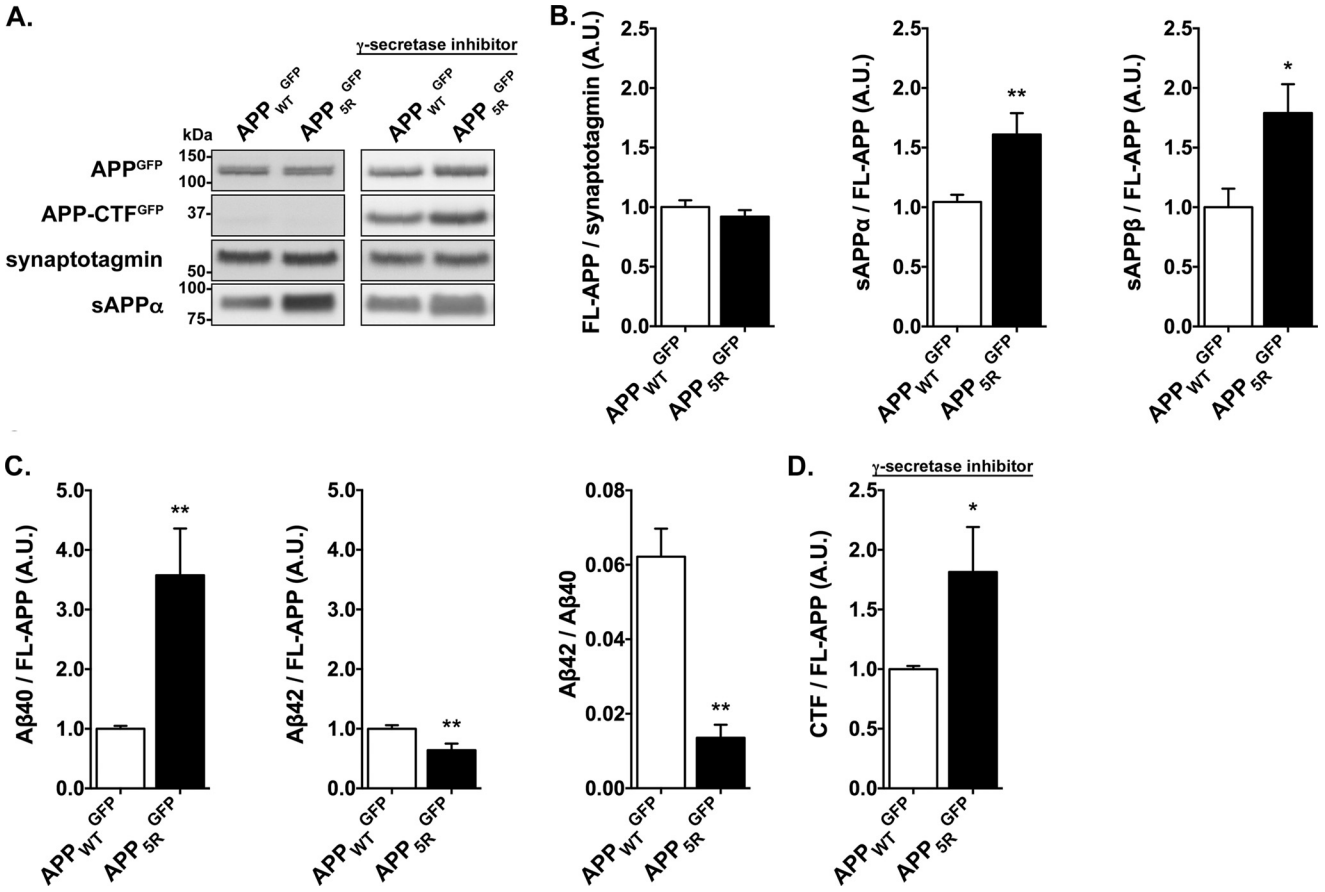

Figure 4. Metabolism of APP_{5R}^{GFP} mutant in primary neurons shows a comparable profile in N2a cells. APP_{WT}^{GFP} or APP_{5R}^{GFP} was expressed in primary murine cortical neurons via lentivirus at DIV 7, and cell lysate and culture media were harvested at DIV 14. γ-Secretase inhibitor XXI was applied at 2 μM to indicated samples for 24 h before harvest. *A,* representative Western blot of full-length APP^{GFP} (FL-APP^{GFP}) and synaptotagmin1 from cell lysate and sAPPα from cell media. *B,* quantification of FL-APP^{GFP} and sAPPα from Western blot, and quantification of sAPPβ by ELISA of cell culture media. FL-APP^{GFP} is normalized to synaptotagmin1 loading control, and sAPPα and sAPPβ are normalized to FL-APP^{GFP}. *C,* quantification of Aβ40 and Aβ42 levels measured by ELISA and normalized to FL-APP^{GFP} and ratio of Aβ42/Aβ40. *D,* quantification of APP C-terminal fragment (APP-CTF^{GFP}), normalized to FL-APP^{GFP} in cells treated with γ-secretase inhibitor XXI. All are expressed in arbitrary units (*A.U.*) relative to APP_{WT}^{GFP}. Values denote mean ± S.E., $n = 7–17$ total number of samples in four separate experimental dissections (three dissections in *D*). *, $p < 0.05$; **, $p < 0.01$, as measured by Student's *t* test.

brane. Ubiquitin is a known signal for ESCRT, which is responsible for sorting cargo into ILVs of MVEs (35). As shown previously, APP is a cargo of ESCRT, and APP_{3R} accumulates on the endosomal limiting membrane instead of being sorted onto ILVs (7). To determine endosomal localization of APP_{5R}^{GFP}, we co-expressed APP^{GFP} with $Rab5_{Q79L}^{mCherry}$, a constitutively active form of Rab5 that has been used as a tool to distinguish endosome-limiting membrane and endosome interior (*i.e.* ILVs) (7, 33, 43, 50). Immunogold electron microscopy labeling in cells that do not express $Rab5_{Q79L}$ and immunofluorescence of naturally occurring large endosomes previously confirmed that endogenous APP is indeed sorted into ILVs of MVEs (7). Here, we show that APP_{5R}^{GFP} is partially redistributed from the endosome ILVs to the endosome-limiting membrane in N2a cells (Fig. 6, *A* and *B*). As amyloidogenic cleavage of APP is thought to occur primarily on the endosomal membrane, prevention of APP sorting into ILVs could increase interaction between APP, BACE1, and γ-secretase, facilitating processing of APP and generation of Aβ. Airyscan confocal microscopy uses a specialized detector array that allows inclusion of the fluorescent signal that would otherwise be rejected by the single confocal pinhole, and it enhances the resolution by a factor of 1.7. Airyscan images of N2a cells expressing APP^{GFP} and $Rab5_{Q79L}^{mCherry}$ show multiple examples of round APP_{WT}^{GFP} vesicles inside enlarged $Rab5_{Q79L}^{mCherry}$ endosomes, which are absent in APP_{5R}^{GFP}-expressing cells and thought to be APP^{GFP} located on ILV membranes (Fig. 6*C*).

Protein cargo sorted onto ILVs can undergo several fates. Two downstream pathways of ILVs include degradation of ILVs and cargo via the lysosome or extracellular release of ILVs as exosomes. The missorting of APP_{5R} led us to hypothesize that one or both of these downstream pathways could be affected. To determine whether lack of APP ILV sorting would affect degradation of FL-APP or APP-CTFs, we inhibited protein synthesis with cycloheximide (CHX) and chased the levels of each over time (Fig. 7, *A* and *B*). Because the APP-CTFs are rapidly degraded by γ-secretase, we applied a γ-secretase inhibitor to identify differences in APP-CTF degradation that are not due to γ-secretase cleavage. We did not detect any differences in FL-APP or APP-CTF degradation between APP_{WT} and APP_{5R}. By adding endolysosomal proton pump inhibitor bafilomycin A1 to specifically examine changes in lysosomal degradation, we again noted no difference in degradation of APP_{WT} and APP_{5R} (Fig. 7, *C* and *D*). Thus, the increase in APP

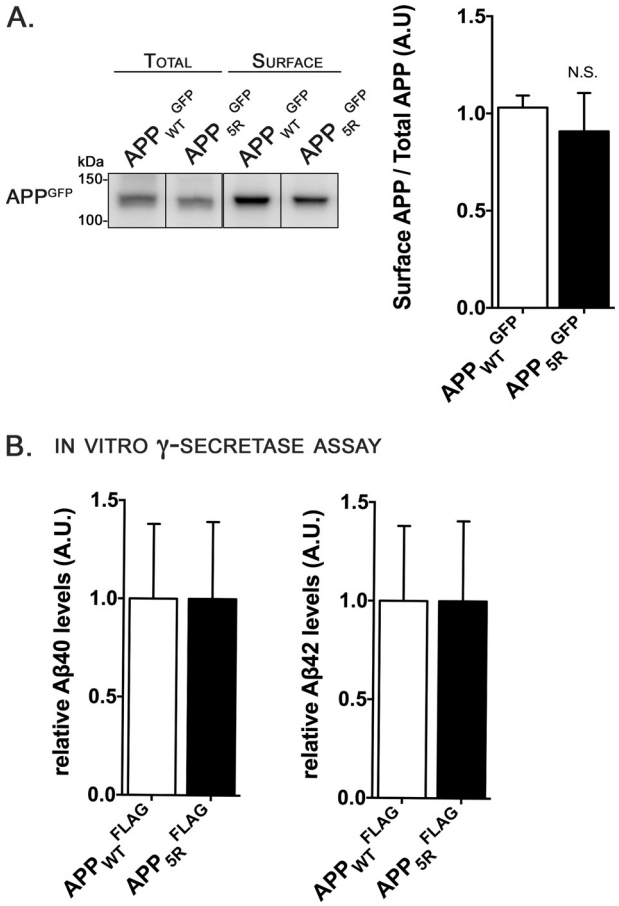

Figure 5. APP_{5R} does not accumulate on cell surface, and γ-secretase cleavage does not produce more Aβ40 from APP_{5R} in a cell-free assay. *A,* representative Western blot of total and surface APP^{GFP} from N2a cells expressing $APP_{WT}{}^{GFP}$ or $APP_{5R}{}^{GFP}$ with quantification of Western blot, expressed as a fraction of surface to total APP^{GFP}. Values are expressed in arbitrary units (*A.U.*) relative to $APP_{WT}{}^{GFP}$ and denote mean ± S.E., $n = 5$ biological replicates. *N.S.* denotes no significance between samples means, as measured by Student's *t* test. *B,* levels of Aβ40 and Aβ42 from *in vitro* γ-secretase assay. Purified APP C99 substrate is incubated with purified γ-secretase membranes, and resultant Aβ levels are measured via ELISA. Aβ levels are expressed in arbitrary units (*A.U.*) relative to $C99_{WT}$. Values denote mean ± S.E., $n = 6$ biological replicates. No significance between samples means, as measured by Student's *t* test.

processing of APP_{5R} is not largely due to a disruption of APP lysosomal degradation.

The disrupted ILV sorting of ubiquitin-deficient APP mutants led us to suspect that the APP content on exosomes may also be diminished. Exosomes are small extracellular vesicles that are secreted from cells upon fusion of MVEs with the plasma membrane and release of ILVs contained within. Protein cargo sorted into ILVs can be released on exosomes, including APP and APP-CTFs (51–53). To determine whether the disrupted ILV sorting of $APP_{5R}{}^{GFP}$ leads to a deficiency of APP on exosomes, we expressed the APP^{GFP} mutants in N2a cells and then collected and purified exosomes from the cell culture media (Fig. 8*A* and as characterized in Ref. 54). Compared with APP-$CTF_{WT}{}^{GFP}$, APP-$CTF_{5R}{}^{GFP}$ is significantly reduced in exosomes (Fig. 8*B*), consistent with a reduced ability of the mutant to be sorted into ILVs. Levels of Aβ associated with exosomes, as measured by ELISA, reveal a trend for an increase in the levels of Aβ40 associated with exosomes from $APP_{5R}{}^{GFP}$-expressing cells, but not Aβ42. There was a significant decrease in the Aβ42/40 ratio associated with exosomes for $APP_{5R}{}^{GFP}$ (Fig. 8*C*), similar to the profile of secreted Aβ in the media. We note that the ratio of $CTF^{GFP}/AICD^{GFP}$ is different for APP_{WT} compared with APP_{5R}, which may indicate that mutation of AICD lysines changes its stability, because it is already known that the GFP tag artificially stabilizes AICD (55). However, establishing the effects of lysine mutation on AICD will require further investigation.

PSEN2 cleaves missorted APP, leading to Aβ40 increase

The γ-secretase complex is composed of four proteins that are necessary to form a functional enzyme complex: nicastrin, anterior pharynx defective 1 (APH1) A or B/C, presenilin enhancer 2 (PEN-2), and the catalytic subunit presenilin (PSEN) 1 or 2 (56, 57). A recent paper by Sannerud *et al.* (43) suggested that the subcellular localization of PSEN1 and PSEN2 is vastly different. Specifically, they localized PSEN2 to the limiting membrane of the endosome, reminiscent of $APP_{5R}{}^{GFP}$ endosomal localization. We hypothesized that the increase in Aβ40 generated by APP_{5R} may be due to increased cleavage by PSEN2-containing γ-secretase complexes. To test this hypothesis, we successfully knocked down PSEN2 in N2a cells via siRNA (Fig. 9, *A* and *B*), and we observed that the $APP_{5R}{}^{GFP}$-mediated increase in Aβ40 is abolished (Fig. 9, *C* and *D*). Sannerud *et al.* (43) also show that cleavage by PSEN2-containing complexes leads to an increase in intracellular Aβ. Indeed, we observed that intracellular Aβ40 was increased in cells expressing the APP_{5R} mutant (Fig. 9*E*). Furthermore, PSEN2 depletion in $APP_{5R}{}^{GFP}$-expressing cells abrogated this increase. No significant changes were observed for Aβ42. Collectively, these results corroborate our hypothesis that the higher Aβ40 levels measured in APP_{5R}-expressing cells are due to increased cleavage by PSEN2-containing γ-secretase complexes. Although Sannerud *et al.* (43) showed that PSEN1 contributes more to extracellular Aβ secretion than PSEN2, our data suggest that PSEN2-containing γ-secretase complexes on the endosomal limiting membrane cleave an additional pool of APP-CTF^{GFP} that accumulates when $APP_{5R}{}^{GFP}$ fails to be sequestered in ILVs. Unexpectedly, the reduction in the $APP_{5R}{}^{GFP}$ Aβ42/Aβ40 ratio was unchanged upon PSEN2 depletion, although there was a greater and more significant reduction in the $APP_{WT}{}^{GFP}$ condition. To confirm the specific role of PSEN2 in the increased secretion of $APP_{5R}{}^{GFP}$ Aβ40, we successfully knocked down PSEN1 in N2a cells using siRNA (supplemental Fig. S1, *A* and *B*). However, PSEN1 depletion led to a compensatory increase in PSEN2 that was significant for $APP_{5R}{}^{GFP}$ only, which complicated interpretation of any changes in levels of Aβ. Nonetheless, the depletion of PSEN1 did not lead to a significant reduction in Aβ40 in $APP_{5R}{}^{GFP}$-expressing cells (37.3 ± 11.3% increase in Aβ40 in control-treated cells compared with a 14.1 ± 9.0% increase in PSEN1-depleted cells; $p = 0.004$ and 0.372, respectively), as it did upon depletion of PSEN2. However, PSEN1 depletion did abolish the difference in Aβ40 between $APP_{WT}{}^{GFP}$- and $APP_{5R}{}^{GFP}$-expressing cells, which may be due to an overall decrease in γ-secretase activity and reflect the large contribution of PSEN1 to cleavage of APP. Consistent with our hypothesis, the increase in intracellular

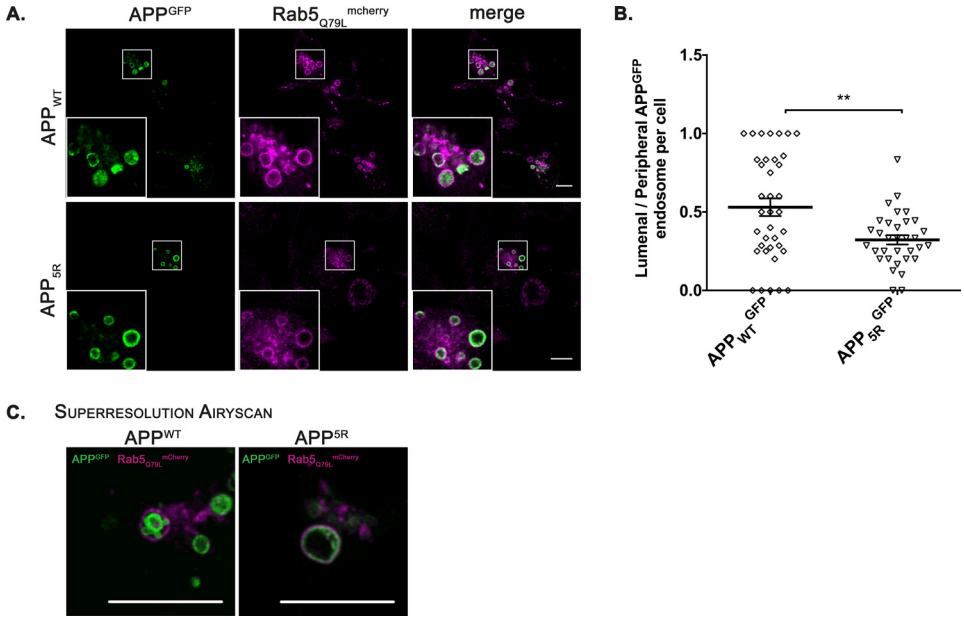

Figure 6. APP_{5R} is mislocalized to the endosome-limiting membrane. *A,* representative confocal images of endosomes in N2a cells expressing APP_{WT}^{GFP} or APP_{5R}^{GFP} and $Rab5_{Q79L}^{mCherry}$. *Scale bar,* 10 μm. *B,* quantification of APP^{GFP} localization in the endosome by enumerating proportion of endosomes with GFP signal luminally to peripherally, per cell. Values denote mean $\pm$ S.E., $n = 29–37$ cells from three separate experiments. **, $p < 0.01$, as measured by Student's *t* test. *C,* super-resolution Airyscan images of endosomes in N2a cells expressing APP_{WT}^{GFP} or APP_{5R}^{GFP} and $Rab5_{Q79L}^{mCherry}$ show ILV-like structures within endosomes expressing APP_{WT}^{GFP}. *Scale bar,* 10 μm.

Aβ40 in APP_{5R}^{GFP}-expressing cells is unchanged upon PSEN1 depletion (63.2 $\pm$ 17.5% increase in Aβ40 in control-treated cells compared with a 77.7 $\pm$ 15.0% increase in PSEN1-depleted cells; $p = 0.002$ and $p < 0.0001$ respectively), suggesting that PSEN2 is also more important for the intracellular accumulation of Aβ40 in this mutant. Thus, our data suggest that the specific increase in Aβ40 exhibited by APP_{5R}^{GFP} is primarily due to cleavage of APP_{5R}^{GFP} by PSEN2-containing γ-secretase complexes subsequent to endosomal redistribution of the ubiquitin-deficient APP mutant.

Discussion

Endosomes have been subject to increasingly intense focus in understanding AD pathophysiology because subtle alterations in endosomal sorting can have important implications for the intracellular itinerary of APP and thus its amyloidogenic cleavage (9, 18). We initially implicated APP as a cargo of the ESCRT pathway after an investigation into lipid changes in the AD brain and the discovery of a specific reduction in the endosomal bioactive lipid phosphatidylinositol 3-phosphate (PI3P) that was common to both FAD mouse models and human AD brains in areas associated with AD pathology (7, 58). PI3P is a master regulator of endosomal signaling and binds to hepatocyte growth factor-regulated tyrosine kinase substrate, a component of the ESCRT-0 complex, via its FYVE (Fab-1, YGL023, Vps27, and EEA1) domain. Others have recognized a connection between APP and ESCRT (32, 33), and mutation of an ESCRT-III component, charged multivesicular body protein 2B (CHMP2B), is associated with frontotemporal dementia (59). However, it remains unclear whether ESCRT disruption increases or decreases Aβ generation, and the study of intracellular levels of Aβ has not been consistently performed, although it might represent an important aspect of AD pathogenesis (32, 33). As opposed to altering levels of ESCRT components, which are responsible for normal endosomal sorting of numerous transmembrane cargos, we instead investigated the effects of APP lysine-to-arginine mutants that cannot undergo sorting into ILVs via the ESCRT pathway.

Previous investigators have shown that APP can be ubiquitinated at several residues in the C-terminal domain, as discussed above (7, 36, 37, 39–41). However, the role of APP ubiquitination in the secretory pathway remains unclear. We previously identified a string of three juxtamembrane lysines in the APP C-terminal domain, mutation of which leads to a deficiency of APP ubiquitination in HeLa cells with subsequent redistribution of APP to the limiting membrane of the endosome and selective increase in Aβ40 in primary neuronal cultures (7). BACE1 and components of the γ-secretase complex can also be ubiquitinated. γ-Secretase ubiquitination has been studied in the context of the ubiquitin–proteasome system, as opposed to cellular trafficking, although some evidence suggests that ubiquilin and the proteasome are responsible for presenilin endoproteolysis (60, 61). BACE1 is ubiquitinated at a single lysine in the C terminus, leading to accumulation of BACE1 in endosomes and an increase in APP processing (62). Aβ levels can be reduced by depletion of the deubiquitinase ubiquitin-specific protease 8 (USP8), which increases BACE1 ubiquitination and leads to a redistribution of BACE1 away from Rab11-positive recycling endosomes (63). These studies underline the effect that ubiquitin regulators can have on Aβ production and the need for identification of ubiquitin ligases and deubiquitinases affecting APP itself. This study is an important development beyond our previous work, thanks to growing evidence that the C-terminal two lysine residues of APP can also be ubiquitinated, as discussed in the Introduction. Although our

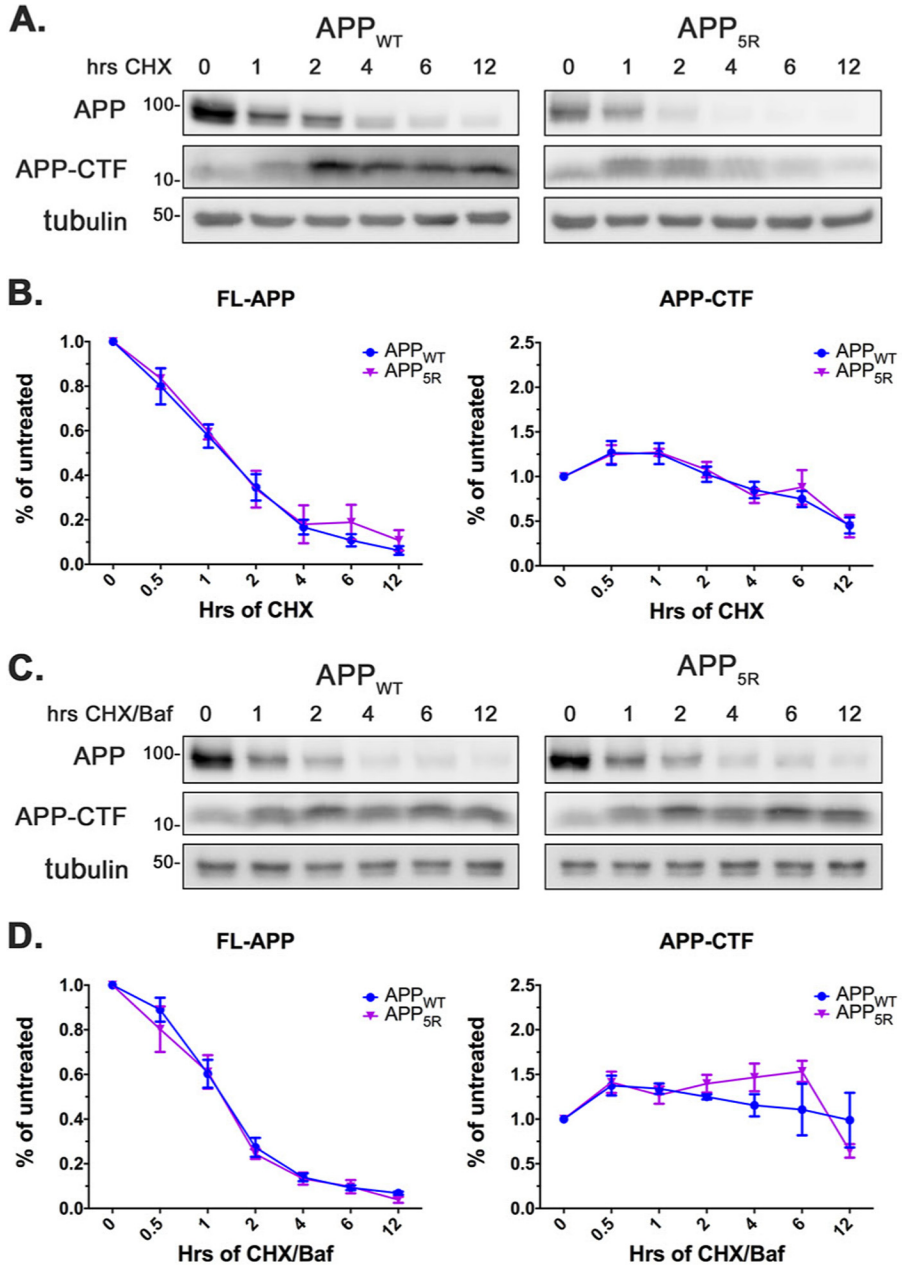

Figure 7. Time course of APP degradation is largely unchanged by APP$_{5R}$ mutation. *A,* representative Western blot of full-length APP (FL-APP), APP C-terminal fragment (APP-CTF), and tubulin at time points of degradation, in the presence of 100 μg/ml CHX and 2 μM γ-secretase inhibitor XXI in N2a cells expressing APP. *B,* quantification of FL-APP and APP-CTF Western blot, expressed as fraction of untreated 0 time point. *C,* representative Western blot of FL-APP, APP-CTF, and tubulin at time points of degradation, in the presence of CHX, γ-secretase inhibitor XXI, and 50 nM bafilomycin A1 (*baf*) in N2a cells expressing APP. *D,* quantification of FL-APP and APP-CTF Western blot, expressed as percent of untreated 0 time point. Values denote mean ± S.E., n = 3–5 biological replicates, and are non-significant as measured by ANOVA with Bonferroni correction.

results here are predominantly consistent with those previously published in Morel *et al.* (7), we show here that N2a cells expressing APP$_{3R}^{GFP}$ exhibit an increase in levels of sAPPα, whereas our prior results do not show such an increase in primary neurons expressing APP$_{3R}^{GFP}$. Although we have no clear explanation for this discrepancy between cell types, we speculate that expression levels may be a key factor. Expression in primary neurons with lentivirus is typically lower (and closer to endogenous levels) than what is achieved with transient transfections in cell lines. Importantly, the key results are congruent between our previous results on APP$_{3R}$ and our current data on APP$_{5R}$, namely the selective increase in Aβ40 for both.

The increase in ubiquitinated APP immunoprecipitated from N2a cells expressing APP$_{WT}^{GFP}$ with co-expression of Ub$_{K48R}^{HA}$ *versus* deubiquitinase-resistant Ub$_{L73P}^{mCherry}$ suggests that the pool of ubiquitinated APP is small or rapidly turned over. This is consistent with our inability to capture sufficient amounts of ubiquitinated APP to assess the ubiquitin chain types decorating the APP cytodomain. Recent work on misfolding-associated protein secretion showed that cells make a concerted effort to remove ubiquitin from quality control substrates prior to secretion and that similar systems could make it difficult to see accumulation of modified APP (64). The APP$_{5R}^{GFP}$ mutant shows a significant reduction of ubiquitina-

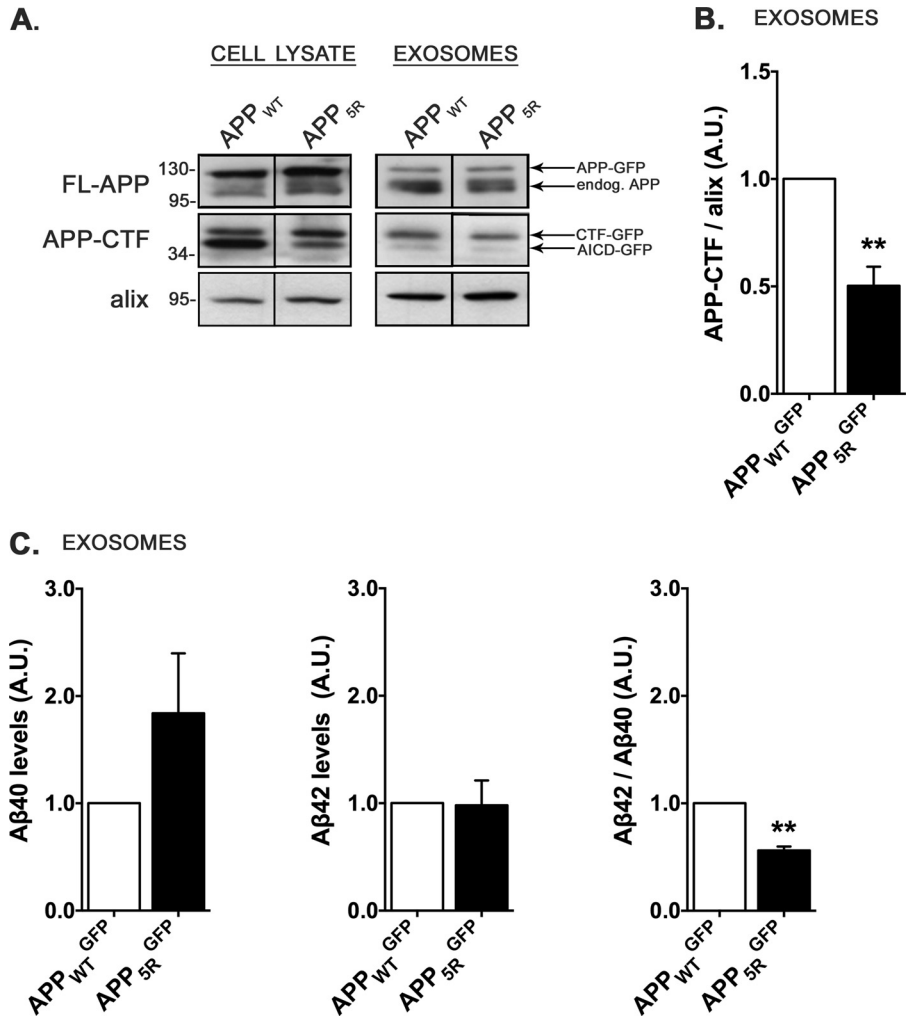

Figure 8. Exosomal content of APP-CTF is reduced in N2a cells expressing APP_{5R}^{GFP}. *A,* representative Western blot of full-length APP (FL-APP, 22C11 N-terminal marker), APP C-terminal fragment (APP-CTF^{GFP}, CT-20 C-terminal marker), and Alix in the cell lysate and exosomes purified by ultracentrifugation of cell media from N2a cells expressing APP^{GFP}. Bands corresponding to exogenous APP^{GFP}, endogenous murine APP, and exogenous APP-CTF^{GFP} and APP intracellular domain (AICD^{GFP}) are indicated by *arrows*. *B,* quantification of APP-CTF^{GFP} in exosomes isolated from cell culture media of N2a cells expressing APP^{GFP}. APP-CTF^{GFP} levels are normalized to Alix, a marker of exosomes, and expressed in arbitrary units (*A.U.*) relative to APP_{WT}^{GFP}. Values denote mean ± S.E., $n = 5$ biological replicates. *C,* Aβ40 and Aβ42 associated with exosomes isolated from cell culture media of N2a cells expressing APP^{GFP} as measured by ELISA. Values are expressed in arbitrary units (*A.U.*) relative to APP_{WT}^{GFP}. Values denote mean ± S.E., $n = 4$ biological replicates. **, $p < 0.01$, as measured by one-sample Student's *t* test.

tion in $Ub_{L73P}^{mCherry}$-expressing cells, and there is a clear effect of lysine mutation. Nonetheless, we cannot rule out at this point a contribution from other post-translational modifications that occur at lysines such as SUMOylation, neddylation, or acetylation (65). Importantly, chemically inducing a physical interaction between ubiquitin and the APP cytodomain was sufficient to decrease the levels of secreted Aβ, even though the ubiquitin modification was at the distal end of APP, suggesting that the specific location of ubiquitination sites may not be as critical as the extent of ubiquitination present on the cytodomain.

Deficiency of APP ubiquitination also impacts the exosomal content of APP and its metabolites, with implications for AD pathology. The role of exosomes in neurodegenerative disease is unclear, but some suggest that they may play a role in the spread of pathology, by carrying misfolded proteins from one cell to another (66). Aβ can be found associated with neuronal exosomes, and along with APP-CTFs, they are increased in exosomes from AD brains (52, 67, 68). Exosomes may also represent a protective element, whereby neuronal exosomes with abundant glycophospholipids could capture extracellular Aβ and prevent subsequent synaptic or neuronal damage (69). The APP_{5R}^{GFP} mutant is not efficiently sorted to ILVs, and thus we see a reduction of APP-CTF on exosomes. Conceivably, this could have implications for the spread of APP fragments, including a reduction of APP-CTF and Aβ spread. However, the role of exosomes in neurodegenerative disease is a growing field, and it is difficult to make predictions at this early stage.

Although its significance is uncertain, intraneuronal accumulation of Aβ has long been observed to precede AD pathology. Recently, Sannerud *et al.* (43) have provided a link between intracellular Aβ and cleavage by PSEN2-containing γ-secretase complexes that are specifically localized to the late endosomal/lysosome compartment. The study showed that PSEN2 is enriched on the limiting membrane of enlarged endosomes, reminiscent of the localization of APP_{5R}^{GFP}. Moreover, many more genetic FAD mutations have been found in PSEN1 as

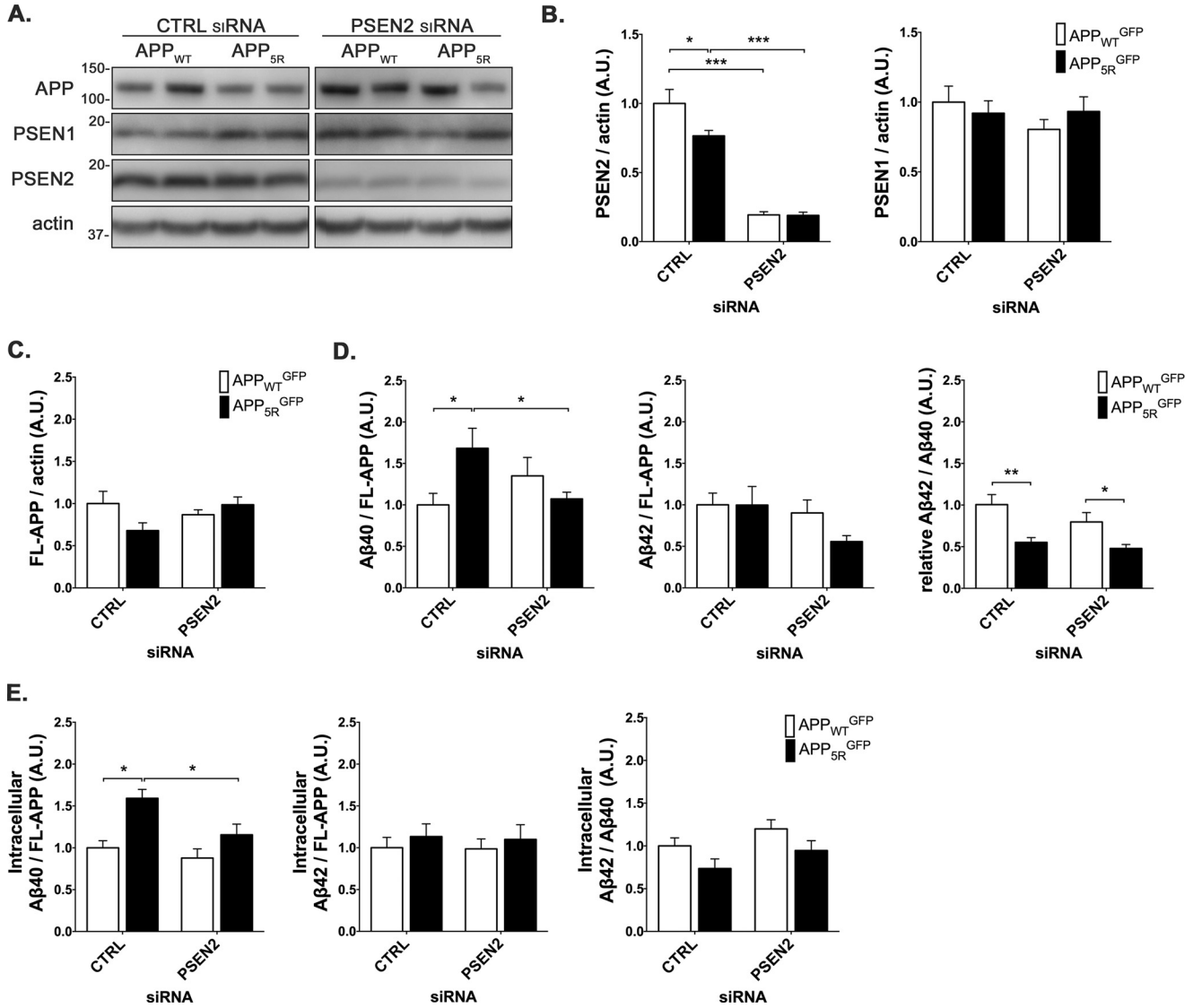

Figure 9. APP$_{5R}$-induced increase in Aβ40 is prevented by presenilin-2 depletion. *A,* representative Western blot of N2a cells treated with non-targeting (*CTRL*) or PSEN2 siRNA and expressing APP^{GFP}. *B,* quantification of Western blot for PSEN1 and PSEN2; *C,* full-length APP (FL-APP), normalized to actin. *D,* secreted Aβ measured by ELISA from culture media, normalized to levels of FL-APP. *E,* intracellular Aβ measured by ELISA of cell lysate, adjusted to protein concentration, and normalized to FL-APP. Values are expressed relative to APP$_{WT}^{GFP}$ control condition, in arbitrary units (*A.U.*). Values denote mean ± S.E., n = 10–13 total samples from four biological replicates. *, $p < 0.05$; **, $p < 0.01$; ***, $p < 0.001$ as measured by two way ANOVA with Bonferroni correction.

opposed to PSEN2. For these reasons, the role of PSEN2 in disease has been largely neglected until recent years. We hypothesized that the increase in APP$_{5R}^{GFP}$-derived Aβ40 is caused by aberrant cleavage of APP-CTF$_{5R}^{GFP}$ that accumulates on the endosomal membrane in proximity to PSEN2. Indeed, depletion of PSEN2 significantly rescues the increase in Aβ40 seen in APP$_{5R}^{GFP}$, both extracellularly and intracellularly to levels of APP$_{WT}^{GFP}$. Although Sannerud *et al.* (43) report an increase in the ratio of Aβ42/40 intracellularly due to PSEN2, we saw the most significant change in levels of Aβ40. This could be due to a difference in cell types or in the particular isoform of APH1 (A or B/C, as well as differently spliced isoforms) in the complex that has been shown to also affect the species of Aβ produced (70–72).

Another recent paper identified a role for CD2AP, a genetic risk factor for LOAD, as a regulator in the sorting of APP from the endosomal limiting membrane to ILVs. Silencing of CD2AP led to an increase in the ratio of Aβ42/40 extracellularly and to an increase in levels of intracellular Aβ42 in dendrites, as measured by immunofluorescence, as well as a deficiency in APP degradation (34). The difference in APP metabolism observed between CD2AP silencing and removal of ubiquitination sites in APP suggests that CD2AP and ubiquitination regulate distinct pathways of ILV sorting, likely with different downstream fates (*i.e.* lysosomal degradation *versus* exosomal sorting, respectively).

The most striking phenotype of the APP$_{5R}$ mutant is the selective increase in Aβ40 and the resulting decrease in the Aβ42/40 ratio. Most FAD mutations lead to an increase in total Aβ production or skew cleavage toward longer, more aggregate-prone species of Aβ thereby increasing the Aβ42/40 ratio, possibly through a partial loss of function in the case of presenilin mutations (14, 73). Selectively increasing Aβ40 is protective against plaque formation by interfering with Aβ42 aggre-

gation (74–77) and may inhibit Aβ42-induced pathology (45). Thus, reducing APP ubiquitination, which leads specifically to an increase in Aβ40, may prevent pathology. However, we must emphasize caution in extending this interpretation *in vivo*, because the main component of amyloid deposits in cerebral amyloid angiopathy appears to be Aβ40, and it is thus unlikely that an excess of Aβ40 produced by decreased APP ubiquitination would be beneficial in this setting (78). These APP lysine-to-arginine mutants are thus perfectly suited to studying the effect of Aβ40 increase *in vivo*. This also has important implications in understanding mechanisms of action of γ-secretase modulators that aim to shift the C-terminal cleavage of Aβ to reduce production of Aβ42, sometimes at the expense of an increase in the relative amount of shorter Aβ species (79, 80).

AD afflicts a growing number of people every year, but clinical trials thus far have been disappointing. Recently, aducanumab has shown some promise in amyloid plaque reduction and slowing cognitive decline, although we await phase 3 clinical trials (81). Elucidating the endosomal trafficking itinerary of APP is crucial for understanding the pathophysiology of AD and why promising new drugs have been ineffective. Furthermore, the recognition of the endosome as a crucial decision point in the amyloidogenic pathway opens the door for discovery of much needed novel therapeutic targets, such as ubiquitin ligases or deubiquitinases.

Experimental procedures

Antibodies and reagents

The antibody against PSEN1 was a kind gift from James J. Lah (Emory University) and Tae Wan Kim (Columbia University). Monoclonal mouse antibodies against APP were 6E10 (Covance SIG-39300), C1/6.1 (BioLegend 802801), 22C11 (Millipore MAB348), and CT-20 (Millipore 171610). Mouse monoclonal antibodies were obtained against the following proteins: GFP (Roche Diagnostics 7.1 and 13.1 mix 11814460001); ubiquitin (Santa Cruz Biotechnology P4D1 sc-8017); synaptotagmin1 (Synaptic Systems 105011); pan-actin (Novus Biologicals NB600–535); and α-tubulin (Sigma T6074). Rabbit polyclonal antibodies were obtained against the following proteins: GFP (Invitrogen A6455); RFP (Rockland 600401379); Alix (Covalab pAB0204); and PSEN2 (Abcam EP1515Y). Pharmacological reagents used were bafilomycin A1 (50 nM Wako 023-11641), γ-secretase inhibitor XXI compound E (2 μM EMD Millipore), cycloheximide (100 μg/ml Sigma C4859), A/C heterodimerizer (2.5 μM Clontech 635057), and MG-132 (20 μM Sigma M7449).

Plasmids

Plasmids were kindly provided by the following sources: Ub73P-mCherry FU-1D/2A plasmid from Clarissa Waites (Columbia University) and pET21b-C100-FLAG backbone for C99 constructs used in *in vitro* γ-secretase assay from Dr. Michael Wolfe (Harvard University). Rab5CA(Q79L)-mCherry was a gift from Sergio Grinstein (Addgene plasmid 35138) (82).

The APP^{GFP} lysine-to-arginine plasmids were generated by QuikChange II XL site-directed mutagenesis (Agilent) following the manufacturer's instructions on base plasmids $APP_{WT}{}^{GFP}$ or $APP_{3R}{}^{GFP}$ pEGFP-N3 plasmids (7) with the following primers and their antisense: APP^{GFP} K724R made with base plasmid $APP_{WT}{}^{GFP}$ and primer 5′-CACCTTGGTGATGCTGAGGAAGAAACAGTACACATCCATTC-3′; APP^{GFP} K725R made with base plasmid $APP_{WT}{}^{GFP}$ and primer 5′-CACCTTGGTGATGCTGAAGAGGAAACAGTACACATCCATTC-3′; APP^{GFP} K726R made with base plasmid $APP_{WT}{}^{GFP}$ and primer 5′-CACCTTGGTGATGCTGAAGAAGAGACAGTACACATCCATTC-3′; APP^{GFP} K751R made with base plasmid $APP_{WT}{}^{GFP}$ and primer 5′-GAGCGCCACCTGTCCAGAATGCAGCAGAACGGCTAC-3′; APP^{GFP} K763R made with base plasmid $APP_{WT}{}^{GFP}$ and primer 5′-GAGCGCCACCTGTCCAGAATGCAGCAGAACGGCTAC-3′; APP^{GFP} K751R + K763R made with base plasmid APP^{GFP} K763R and primer 5′-GAGCGCCACCTGTCCAGAATGCAGCAGAACGGCTAC-3′; APP^{GFP} K724R/K725R/K726R + K751R made with base plasmid $APP_{3R}{}^{GFP}$ and primer 5′-GAGCGCCACCTGTCCAGAATGCAGCAGAACGGCTAC-3′; APP^{GFP} K724R/K725R/K726R + K763R made with base plasmid $APP_{3R}{}^{GFP}$ and primer 5′-GGCTACGAAAATCCAACCTACAGGTTCTTTGAGCAGATGC-3′; APP^{GFP} K724R/K725R/K726R + K751R + K763R ($APP_{5R}{}^{GFP}$) made with base plasmid APP K724R/K725R/K726R_K763R and primer 5′-GAGCGCCACCTGTCCAGAATGCAGCAGAACGGCTAC-3′. Human APP^{GFP} lentiviruses were generated by excising GFP with corresponding APP mutations from pEGFP-N3 with NheI/NotI (New England Biolabs) and ligating the cDNAs into pCDH-CMV-MCSr (System Biosciences) with T4 DNA ligase (New England Biolabs).

Human APP plasmids were generated by excising GFP from APP^{GFP} pEGFP-N3 with corresponding APP mutations using BsrGI/SalI (New England Biolabs), followed by DNA end blunting with T4 DNA polymerase (New England Biolabs) and blunt end ligation with T4 DNA ligase (New England Biolabs).

Human APP C100-FLAG plasmids were generated by PCR amplification of APP^{GFP} pEGFP-N3 vectors with respective APP mutations using forward primer 5′-ACAAAGCTTCTACTTATCGTCATCGTCCTTGTAATCGTTCTGCATCTGCTCAAAGAACTT-3′ and reverse primer 5′-ATATCCTGAGTCATGTCGGAATTCTGCATCCATATGGACGAA-3′ followed by digestion of AKp-3 pET21b-C100-FLAG (kind gift from Michael Wolfe) and PCR fragment with NdeI/HindIII (New England Biolabs) and ligation with T4 DNA ligase (New England Biolabs).

Human APP-DmrA-RFP plasmids were generated by PCR amplification of the DmrA-DmrA-mRFP fragment from pHet-Mem1-mRFP (pC4M-F2E-mRFP) with forward primer 5′-TAATGA GTCGAC GGA GTG CAG GTG GAA ACC ATC-3′ and reverse primer 5′-ACG ACG TAC CAG ACT ACG CAT TGTACA GTC GAG-3′ followed by digest of PCR fragment and APP^{GFP} pEGFP-N3 with BsrGI/SalI (New England Biolabs) and ligation with T4 DNA ligase (New England Biolabs).

siRNA

Control siRNA was ON-TARGETplus non-targeting siRNA #1 (GE Healthcare-Dharmacon D-001810-01-05), siRNA against *Psen1* was ON-TARGET plus mouse *Psen1* (19164) siRNA-SMARTpool (GE Healthcare-Dharmacon L-048761-01-0005), and siRNA against *Psen2* was ON-TARGET plus mouse *Psen2* (19164) siRNA (GE Healthcare-Dharmacon

J-051123-10 and J-051123-12). All siRNAs were applied to N2a cells in 6-well plates via Lipofectamine 3000 following the manufacturer's directions, at a concentration of 25 nM. Cells and culture media were harvested after 3 days.

Cell transfection and lentivirus production

HEK-293T and N2a cells were grown at 37 °C in a 5% humidified CO_2 incubator in DMEM (Invitrogen) and 10% FBS (Life Technologies, Inc.). After 24 h of plating, cells were transfected with DNA using Lipofectamine 2000 or 3000 (Invitrogen) or JetPEI (VWR) for 24–48 h via the manufacturer's directions. Cortical neurons were obtained from P0 mice brains, as described previously (7). Briefly, cortices were separated from brain and dissociated in 2.5% trypsin (Life Technologies, Inc.). Neurons were plated on polyornithine (Sigma)-coated six-well plates and were incubated with minimum Eagle's medium (Invitrogen) with 10% FBS. After 5 h, neurons were transferred into serum-free Neurobasal medium (Life Technologies, Inc.) supplemented with B27 (Invitrogen) + Glutamax (Invitrogen) and cultured for 7 days *in vitro* (DIV). Neurons were infected with lentivirus after 7 days in culture and were cultured up to 14 days. Where indicated, γ-secretase inhibitor was applied 24 h before cell harvest. Lentiviruses were generated by transfecting lentiviral vectors ($APP_{WT}{}^{GFP}$, $APP_{3R}{}^{GFP}$, and $APP_{5R}{}^{GFP}$) into HEK-293T cells using Lipofectamine LTX (Invitrogen). A pPACKH1 packaging mix (System Biosciences) was added to the transfection reagents according to the manufacturer's instructions. The medium was collected 48 and 72 h after transfection, passed through a 45-nm filter, and applied at 1:4 ratio to media.

Fluorescence microscopy

For immunofluorescence experiments, cells grown on glass coverslips were washed once with Hanks' balanced salt solution (Gibco) and fixed with 4% paraformaldehyde (Electron Microscopy Sciences) for 20 min at room temperature. Cells were then washed twice in PBS (Boston Bioproducts) and permeabilized with a buffer containing 0.05% saponin (Acros), 5% BSA in PBS for 45 min at 37 °C. They were then incubated with primary antibodies diluted in the buffer for 1 h at room temperature, washed in buffer three times, incubated with fluorescent secondary antibodies (Invitrogen) diluted in buffer for 1 h at room temperature, and washed again three times in buffer. Cells were finally washed once with PBS, and coverslips were mounted in Vectashield mounting medium (Vector Laboratories). Images were acquired by confocal laser-scanning microscopy (Zeiss LSM 700 and 800) and analyzed with Zeiss Zen and ImageJ software.

Protein biochemistry and immunoblotting

To detect ubiquitinated APP, HEK-293T cells were transiently transfected with human APP^{GFP} and $Ub_{K48R}{}^{HA}$ and then lysed for 30 min at 4 °C in IP buffer (0.5% Nonidet P-40, 500 mM Tris-HCl, pH 7.4, 20 mM EDTA, 10 mM NaF, and a mixture of protease and phosphatase inhibitors (Roche Diagnostics)), and centrifuged for 15 min at 13,000 rpm. Supernatants were diluted to equal concentration and pre-cleared with protein G-Sepharose beads (GE Healthcare) before an overnight incubation at 4 °C with 4 μg of anti-GFP mAβ and a subsequent 2-h incubation at 4 °C with protein G-Sepharose beads. After extensively washing the beads with IP buffer, proteins were eluted, separated on a 4–12% BisTris gel (Invitrogen), and transferred by iBlot (Invitrogen) on a nitrocellulose membrane. Separate membranes were probed with anti-ubiquitin or anti-GFP antibodies. Images were acquired via the LAS4000 imager (GE Healthcare), and quantification was done using ImageJ. For all other immunoblots, cells were lysed for 30 min at 4 °C in Thermo Fisher Scientific RIPA buffer or Pierce IP buffer with protease and phosphatase inhibitor mixtures and centrifuged for 15 min at 13,000 rpm, and proteins in the supernatant were processed for SDS-PAGE and immunoblotting. Tricine 10–20% gels were used for experiments measuring APP-CTFs, and 4–12% BisTris gels were used for all other experiments (Invitrogen). For analysis of exosomes and lysates by Western blotting, exosomes secreted by N2a cells (two dishes of 70 cm^2, ~28 μg of protein) were loaded in parallel to 70 μg of protein lysates, *i.e.* 2% of a total dish. 8% acrylamide glycine gels and electrophoresis in glycine buffer were performed to detect APP^{GFP}, CTF^{GFP}, and Alix. Semi-dry transfer of proteins was done on 0.45-μm PVDF membranes (Millipore) for 1 h. Membranes were blocked in 3% skimmed milk in Tris-buffered saline with 0.01% Tween (TBS/Tween) and incubated with primary antibodies in the blocking solution for 1 h at room temperature or overnight at 4 °C. HRP-bound secondary antibodies were diluted 1:15,000 in TBS/Tween and incubated 1 h on membranes at room temperature. Detection reagent was homemade using a freshly prepared mix of 50% 250 mM luminol and 50% of 90 mM coumaric acid and 0.015% H_2O_2.

Purification of exosomes from N2a cells

Exosomes were isolated as described previously (54) in Mov cells. Exosome-free medium was made by ultracentrifuging complete culture medium at 150,000 × *g* for 18 h followed by sterilization through 0.2-μm filters. 24 h after plating, N2a cells were transfected, and 24 h later complete medium was replaced by exosome-free medium. Cell supernatant was collected after 20 h of secretion, and exosomes were purified by differential ultracentrifugation protocol: 2000 × *g*, 10 min at 4 °C followed by 20,000 × *g*, 30 min at 4 °C. Supernatants were filtered through 0.22-μm Millex GV PVDF filter (Millipore) and finally centrifuged at 110,000 × *g*, 1 h and 30 min at 4 °C in SW41 or SW32 rotors. 110,000 × *g* pellets were resuspended either in sample buffer (2% SDS, 2.5% β-mercaptoethanol, 125 mM Tris-HCl, pH 6.8, 10% glycerol, 2.5% bromphenol blue) for Western blot analysis or in lysis buffer (20 mM Tris, 150 mM NaCl, 1 mM EDTA, 1% Nonidet P-40, anti-protease mix from Roche Diagnostics) to measure protein concentration before anti-Aβ ELISA. When cell lysate was required, N2a cells were lysed in 1 ml of lysis buffer for 30 min on ice and centrifuged at 20,000 × *g*, 10 min at 4 °C before use.

Cell surface biotinylation assay

Components of the Pierce cell-surface protein isolation kit (Thermo Fisher Scientific 89881) were used with modifications to the kit protocol. N2a cells were grown in 6-well plates, transfected with APP^{GFP}, and harvested after 24 h. Plates were

washed with PBS on ice and incubated with biotin for 30 min at 4 °C and then with quenching solution for 5 min at 4 °C. Cells were then washed with TBS, scraped into 100 μl of Pierce IP lysis buffer, sonicated five times for 1 s on a low setting, and centrifuged at 10,000 × *g* for 2 min at 4 °C. A sample of the total lysate was saved for Western blot analysis, and the remaining was incubated with bead slurry (50% washed beads, 50% lysis buffer) for 1 h at 4 °C. Beads were collected by centrifugation, washed three times in wash buffer, and diluted in sample buffer and reducing agent for further SDS-PAGE and immunoblotting analysis.

γ-Secretase assay

APP_{WT} and APP_{5R} C100-FLAG substrates (APP C99 with an N-terminal methionine and a C-terminal FLAG tag) were expressed in BL21-CodonPlus cells (Agilent) and purified using M2 anti-FLAG affinity gel (Sigma). The protein concentration in each C100-FLAG preparation was measured by BCA assay (Pierce). 1 μM substrate was incubated with purified γ-secretase from S20 cell line (CHO cells expressing four γ-secretase components, including PSEN1) in assay buffer (50 mM HEPES, pH 7.0, and 150 mM NaCl) with 0.1% phosphatidylcholine, 0.025% phosphatidylethanolamine, 0.00625% cholesterol, and 0.25% CHAPSO for 1 h at 37 °C. Aβ40 and Aβ42 generated in the reactions were quantified using specific ELISAs (Invitrogen).

Chemically induced ubiquitination assay

DNA constructs and heterodimerizer agent were used from the commercially available iDimerize Inducible Heterodimerizer System (Clontech). N2a cells at 60% confluence in 10-cm plates were transfected with $APP_{WT}^{DmrA\text{-}RFP}$ or $APP_{5R}^{DmrA\text{-}RFP}$ alone or co-transfected with Ub^{DmrC}. Culture media were changed 24 h after transfection, and ethanol or 2.5 μM A/C heterodimerizer dissolved in ethanol were added as indicated. Culture media and cells were harvested as described above, 12 h after media change, to measure Aβ40 and Aβ42 levels via ELISA.

Enzyme-linked immunosorbent assays

To measure human Aβ40 and Aβ42, or human sAPPβ from cell culture of N2a cells transfected with APP^{GFP}, media were changed 24 h before cell harvest. For cortical neuronal cultures expressing APP^{GFP}, media were collected at DIV 14, 7 days after application of lentivirus. Media were collected at 4 °C and supplemented with 0.25 mg/ml Pefabloc SC 4-(2-aminoethyl)benzenesulfonyl fluoride hydrochloride (Fuka Analytical) and centrifuged at low speed to remove cell debris for 5 min. Intracellular Aβ40 and Aβ42 was measured from cells lysed for 30 min in 20 mM Tris, pH 7.4, 150 mM NaCl, 1 mM EDTA, 1% Nonidet P-40, and protease and phosphatase inhibitor mixtures at 4 °C and then centrifuged at 13,000 rpm for 15 min. Thermo Fisher Scientific (Invitrogen) ELISA kits were used for Aβ40 and Aβ42 measurements from cell culture media and *in vitro* γ-secretase assay. Mesoplex V-PLEX Aβ Peptide Panel 1 (4G8) kits (Meso Scale Discovery) were used for Aβ40 and Aβ42 measurements from cell lysate and exosomes, where an equal concentration of protein, measured by BCA assay (Pierce), was loaded for each sample. Covance kits were used for measurements of sAPPβ from cell culture media. All kits were used according to the manufacturer's instructions.

Statistics

Statistical analysis was performed using GraphPad Prism software (version 6). All mutant samples were compared with WT using the two-tailed Student's *t* test (for the comparison of two averages) and the one-sample *t* test (for the comparison of one average to a normalized value where variability is lost). A one-tailed *t* test was exceptionally used in Fig. 1 based on similar experiments in previous studies (7). Two-way ANOVA was used for APP degradation experiment and PSEN2 knockdown experiment.

Author contributions—R. L. W. designed, coordinated, and carried out the bulk of the experiments. K. L. isolated exosomes from N2a cells and characterized them via Western blotting. A. M. M. assisted with exosome characterization and Aβ measurements. M. A. F. carried out the *in vitro* γ-secretase assay. R. L. W., K. L., A. M. M., M. A. F., M. S. W., R. S., and G. D. P. edited the manuscript. R. L. W. and G. D. P. wrote the manuscript. G. D. P. conceived the project and supervised the study. All authors reviewed the results and approved the final version of the manuscript.

Acknowledgments—We are grateful to Dr. Clarissa Waites for the kind gift Ub73P-mCherry FU-1D/2A plasmid, Dr. Sergio Grinstein for the Rab5CA(Q79L)-mCherry plasmid, and Drs. Tae-Wan Kim and James J. Lah for the presenilin 1 antibody. We are grateful for critical review of the manuscript by Drs. Donald Kirkpatrick, Catherine Marquer, and Scott Small. We also thank Drs. Clarissa Waites and Samuel Gandy for helpful discussions.

References

1. Selkoe, D. J., and Hardy, J. (2016) The amyloid hypothesis of Alzheimer's disease at 25 years. *EMBO Mol. Med.* **8,** 595–608
2. Rajendran, L., and Annaert, W. (2012) Membrane trafficking pathways in Alzheimer's disease. *Traffic* **13,** 759–770
3. Haass, C., Kaether, C., Thinakaran, G., and Sisodia, S. (2012) Trafficking and proteolytic processing of APP. *Cold Spring Harb. Perspect. Med.* **2,** a006270
4. Cirrito, J. R., Kang, J. E., Lee, J., Stewart, F. R., Verges, D. K., Silverio, L. M., Bu, G., Mennerick, S., and Holtzman, D. M. (2008) Endocytosis is required for synaptic activity-dependent release of amyloid-β *in vivo*. *Neuron* **58,** 42–51
5. Zou, L., Wang, Z., Shen, L., Bao, G. B., Wang, T., Kang, J. H., and Pei, G. (2007) Receptor tyrosine kinases positively regulate BACE activity and amyloid-β production through enhancing BACE internalization. *Cell Res.* **17,** 389–401
6. Sannerud, R., Declerck, I., Peric, A., Raemaekers, T., Menendez, G., Zhou, L., Veerle, B., Coen, K., Munck, S., De Strooper, B., Schiavo, G., and Annaert, W. (2011) ADP ribosylation factor 6 (ARF6) controls amyloid precursor protein (APP) processing by mediating the endosomal sorting of BACE1. *Proc. Natl. Acad. Sci. U.S.A.* **108,** E559–E568
7. Morel, E., Chamoun, Z., Lasiecka, Z. M., Chan, R. B., Williamson, R. L., Vetanovetz, C., Dall'Armi, C., Simoes, S., Point Du Jour, K. S., McCabe, B. D., Small, S. A., and Di Paolo, G. (2013) PI3P regulates sorting and processing of amyloid precursor protein through the endosomal system. *Nat. Commun.* **4,** 2250
8. Small, S. A., and Gandy, S. (2006) Sorting through the cell biology of Alzheimer's disease: intracellular pathways to pathogenesis. *Neuron* **52,** 15–31
9. Rajendran, L., Schneider, A., Schlechtingen, G., Weidlich, S., Ries, J., Braxmeier, T., Schwille, P., Schulz, J. B., Schroeder, C., Simons, M., Jen-

nings, G., Knölker, H.-J., and Simons, K. (2008) Efficient inhibition of the Alzheimer's disease β-secretase by membrane targeting. *Science* **320,** 520–523
10. Vassar, R., Bennett, B. D., Babu-Khan, S., Kahn, S., Mendiaz, E. A., Denis, P., Teplow, D. B., Ross, S., Amarante, P., Loeloff, R., Luo, Y., Fisher, S., Fuller, J., Edenson, S., Lile, J., *et al.* (1999) β-Secretase cleavage of Alzheimer's amyloid precursor protein by the transmembrane aspartic protease BACE. *Science* **286,** 735–741
11. Buggia-Prévot, V., Fernandez, C. G., Riordan, S., Vetrivel, K. S., Roseman, J., Waters, J., Bindokas, V. P., Vassar, R., and Thinakaran, G. (2014) Axonal BACE1 dynamics and targeting in hippocampal neurons: a role for Rab11 GTPase. *Mol. Neurodegener.* **9,** 1
12. Das, U., Scott, D. A., Ganguly, A., Koo, E. H., Tang, Y., and Roy, S. (2013) Activity-induced convergence of APP and BACE-1 in acidic microdomains via an endocytosis-dependent pathway. *Neuron* **79,** 447–460
13. Das, U., Wang, L., Ganguly, A., Saikia, J. M., Wagner, S. L., Koo, E. H., and Roy, S. (2016) Visualizing APP and BACE-1 approximation in neurons yields insight into the amyloidogenic pathway. *Nat. Neurosci.* **19,** 55–64
14. Wolfe, M. S. (2012) Processive proteolysis by γ-secretase and the mechanism of Alzheimer's disease. *Biol. Chem.* **393,** 899–905
15. Musiek, E. S., and Holtzman, D. M. (2015) Three dimensions of the amyloid hypothesis: time, space and "wingmen." *Nat. Neurosci.* **18,** 800–806
16. Nixon, R. A. (2005) Endosome function and dysfunction in Alzheimer's disease and other neurodegenerative diseases. *Neurobiol. Aging* **26,** 373–382
17. Gouras, G. K. (2013) Convergence of synapses, endosomes, and prions in the biology of neurodegenerative diseases. *Int. J. Cell Biol.* **2013,** 141083
18. Toh, W. H., and Gleeson, P. A. (2016) Dysregulation of intracellular trafficking and endosomal sorting in Alzheimer's disease: controversies and unanswered questions. *Biochem. J.* **473,** 1977–1993
19. Tosto, G., and Reitz, C. (2013) Genome-wide association studies in Alzheimer's disease: a review topical collection on dementia. *Curr. Neurol. Neurosci. Rep.* **13,** 381
20. Hollingworth, P., Harold, D., Sims, R., Gerrish, A., Lambert, J.-C., Carrasquillo, M. M., Abraham, R., Hamshere, M. L., Pahwa, J. S., Moskvina, V., Dowzell, K., Jones, N., Stretton, A., Thomas, C., Richards, A., *et al.* (2011) Common variants at ABCA7, MS4A6A/MS4A4E, EPHA1, CD33 and CD2AP are associated with Alzheimer's disease. *Nat. Genet.* **43,** 429–435
21. Lambert, J. C., Ibrahim-Verbaas, C. A., Harold, D., Naj, A. C., Sims, R., Bellenguez, C., DeStafano, A. L., Bis, J. C., Beecham, G. W., Grenier-Boley, B., Russo, G., Thorton-Wells, T. A., Jones, N., Smith, A. V., Chouraki, V., *et al.* (2013) Meta-analysis of 74,046 individuals identifies 11 new susceptibility loci for Alzheimer's disease. *Nat. Genet.* **45,** 1452–1458
22. Bohm, C., Chen, F., Sevalle, J., Qamar, S., Dodd, R., Li, Y., Schmitt-Ulms, G., Fraser, P. E., and St George-Hyslop, P. H. (2015) Current and future implications of basic and translational research on amyloid-β peptide production and removal pathways. *Mol. Cell. Neurosci.* **66,** 3–11
23. Peric, A., and Annaert, W. (2015) Early etiology of Alzheimer's disease: tipping the balance toward autophagy or endosomal dysfunction? *Acta Neuropathol.* **129,** 363–381
24. Muhammad, A., Flores, I., Zhang, H., Yu, R., Staniszewski, A., Planel, E., Herman, M., Ho, L., Kreber, R., Honig, L. S., Ganetzky, B., Duff, K., Arancio, O., and Small, S. A. (2008) Retromer deficiency observed in Alzheimer's disease causes hippocampal dysfunction, neurodegeneration, and Aβ accumulation. *Proc. Natl. Acad. Sci. U.S.A.* **105,** 7327–7332
25. Small, S. A., Kent, K., Pierce, A., Leung, C., Kang, M. S., Okada, H., Honig, L., Vonsattel, J. P., and Kim, T. W. (2005) Model-guided microarray implicates the retromer complex in Alzheimer's disease. *Ann. Neurol.* **58,** 909–919
26. Small, S. A., and Petsko, G. A. (2015) Retromer in Alzheimer disease, Parkinson disease and other neurological disorders. *Nat. Rev. Neurosci.* **16,** 126–132
27. Bhalla, A., Vetanovetz, C. P., Morel, E., Chamoun, Z., Di Paolo, G., and Small, S. A. (2012) The location and trafficking routes of the neuronal retromer and its role in amyloid precursor protein transport. *Neurobiol. Dis.* **47,** 126–134
28. Oddo, S., Caccamo, A., Shepherd, J. D., Murphy, M. P., Golde, T. E., Kayed, R., Metherate, R., Mattson, M. P., Akbari, Y., and LaFerla, F. M. (2003) Triple-transgenic model of Alzheimer's disease with plaques and tangles: intracellular Aβ and synaptic dysfunction. *Neuron* **39,** 409–421
29. Gouras, G. K., Tampellini, D., Takahashi, R. H., and Capetillo-Zarate, E. (2010) Intraneuronal β-amyloid accumulation and synapse pathology in Alzheimer's disease. *Acta Neuropathol.* **119,** 523–541
30. Takahashi, R. H., Milner, T. A., Li, F., Nam, E. E., Edgar, M. A., Yamaguchi, H., Beal, M. F., Xu, H., Greengard, P., and Gouras, G. K. (2002) Intraneuronal Alzheimer Aβ42 accumulates in multivesicular bodies and is associated with synaptic pathology. *Am. J. Pathol.* **161,** 1869–1879
31. Takahashi, R. H., Almeida, C. G., Kearney, P. F., Yu, F., Lin, M. T., Milner, T. A., and Gouras, G. K. (2004) Oligomerization of Alzheimer's β-amyloid within processes and synapses of cultured neurons and brain. *J. Neurosci.* **24,** 3592–3599
32. Choy, R. W., Cheng, Z., and Schekman, R. (2012) Amyloid precursor protein (APP) traffics from the cell surface via endosomes for amyloid β (Aβ) production in the trans-Golgi network. *Proc. Natl. Acad. Sci. U.S.A.* **109,** E2077–E2082
33. Edgar, J. R., Willén, K., Gouras, G. K., and Futter, C. E. (2015) ESCRTs regulate amyloid precursor protein sorting in multivesicular bodies and intracellular amyloid-β accumulation. *J. Cell Sci.* **128,** 2520–2528
34. Ubelmann, F., Burrinha, T., Salavessa, L., Gomes, R., Ferreira, C., Moreno, N., and Guimas Almeida, C. (2017) Bin1 and CD2AP polarise the endocytic generation of β-amyloid. *EMBO Rep.* **18,** 102–122
35. MacGurn, J. A., Hsu, P.-C., and Emr, S. D. (2012) Ubiquitin and membrane protein turnover: from cradle to grave. *Annu. Rev. Biochem.* **81,** 231–259
36. Watanabe, T., Hikichi, Y., Willuweit, A., Shintani, Y., and Horiguchi, T. (2012) FBL2 regulates amyloid precursor protein (APP) metabolism by promoting ubiquitination-dependent APP degradation and inhibition of APP endocytosis. *J. Neurosci.* **32,** 3352–3365
37. Del Prete, D., Rice, R. C., Rajadhyaksha, A. M., and D'Adamio, L. (2016) Amyloid precursor protein (APP) may act as a substrate and a recognition unit for CRL4-CRBN and Stub1 E3 ligases facilitating ubiquitination of proteins involved in presynaptic functions and neurodegeneration. *J. Biol. Chem.* **291,** 17209–17227
38. Tosto, G., Fu, H., Vardarajan, B. N., Lee, J. H., Cheng, R., Reyes-Dumeyer, D., Lantigua, R., Medrano, M., Jimenez-Velazquez, I. Z., Elkind, M. S., Wright, C. B., Sacco, R. L., Pericak-Vance, M., Farrer, L., Rogaeva, E., *et al.* (2015) F-box/LRR-repeat protein 7 is genetically associated with Alzheimer's disease. *Ann. Clin. Transl. Neurol.* **2,** 810–820
39. Kim, W., Bennett, E. J., Huttlin, E. L., Guo, A., Li, J., Possemato, A., Sowa, M. E., Rad, R., Rush, J., Comb, M. J., Harper, J. W., and Gygi, S. P. (2011) Systematic and quantitative assessment of the ubiquitin-modified proteome. *Mol. Cell* **44,** 325–340
40. Wagner, S. A., Beli, P., Weinert, B. T., Nielsen, M. L., Cox, J., Mann, M., and Choudhary, C. (2011) A proteome-wide, quantitative survey of *in vivo* ubiquitylation sites reveals widespread regulatory roles. *Mol. Cell. Proteomics* **10,** M111.013284
41. El Ayadi, A., Stieren, E. S., Barral, J. M., and Boehning, D. (2012) Ubiquilin-1 regulates amyloid precursor protein maturation and degradation by stimulating K63-linked polyubiquitination of lysine 688. *Proc. Natl. Acad. Sci.* **109,** 13416–13421
42. Bustamante, H. A., Rivera-Dictter, A., Cavieres, V. A., Muñoz, V. C., González, A., Lin, Y., Mardones, G. A., and Burgos, P. V. (2013) Turnover of C99 is controlled by a crosstalk between ERAD and ubiquitin-independent lysosomal degradation in human neuroglioma cells. *PLoS ONE* **8,** e83096
43. Sannerud, R., Esselens, C., Ejsmont, P., Mattera, R., Rochin, L., Tharkeshwar, A. K., De Baets, G., De Wever, V., Habets, R., Baert, V., Vermeire, W., Michiels, C., Groot, A. J., Wouters, R., Dillen, K., *et al.* (2016) Restricted location of PSEN2/γ-secretase determines substrate specificity and generates an intracellular Aβ pool. *Cell* **166,** 193–208
44. Kim, J., Onstead, L., Randle, S., Price, R., Smithson, L., Zwizinski, C., Dickson, D. W., Golde, T., and McGowan, E. (2007) Aβ40 inhibits amyloid deposition *in vivo*. *J. Neurosci.* **27,** 627–633
45. Bate, C., and Williams, A. (2010) Amyloid-β(1–40) inhibits amyloid-β(1–42) induced activation of cytoplasmic phospholipase A2 and synapse degeneration. *J. Alzheimer's Dis.* **21,** 985–993

46. Tanno, H., and Komada, M. (2013) The ubiquitin code and its decoding machinery in the endocytic pathway. *J. Biochem.* **153,** 497–504
47. Békés, M., Okamoto, K., Crist, S. B., Jones, M. J., Chapman, J. R., Brasher, B. B., Melandri, F. D., Ueberheide, B. M., Denchi, E. L., and Huang, T. T. (2013) DUB-resistant ubiquitin to survey ubiquitination switches in mammalian cells. *Cell Rep.* **5,** 826–838
48. Crabtree, G. R., and Schreiber, S. L. (1996) Three-part inventions: intracellular signaling and induced proximity. *Trends Biochem. Sci.* **21,** 418–422
49. Clackson, T., Yang, W., Rozamus, L. W., Hatada, M., Amara, J. F., Rollins, C. T., Stevenson, L. F., Magari, S. R., Wood, S. A., Courage, N. L., Lu, X., Cerasoli, F., Jr., Gilman, M., and Holt, D. A. (1998) Redesigning an FKBP-ligand interface to generate chemical dimerizers with novel specificity. *Proc. Natl. Acad. Sci. U.S.A.* **95,** 10437–10442
50. Wegner, C. S., Wegener, C. S., Malerød, L., Pedersen, N. M., Progida, C., Prodiga, C., Bakke, O., Stenmark, H., and Brech, A. (2010) Ultrastructural characterization of giant endosomes induced by GTPase-deficient Rab5. *Histochem. Cell Biol.* **133,** 41–55
51. Vingtdeux, V., Hamdane, M., Loyens, A., Gelé, P., Drobeck, H., Bégard, S., Galas, M.-C., Delacourte, A., Beauvillain, J.-C., Buée, L., and Sergeant, N. (2007) Alkalizing drugs induce accumulation of amyloid precursor protein by-products in luminal vesicles of multivesicular bodies. *J. Biol. Chem.* **282,** 18197–18205
52. Perez-Gonzalez, R., Gauthier, S. A., Kumar, A., and Levy, E. (2012) The exosome-secretory pathway transports amyloid precursor protein carboxyl-terminal fragments from the cell into the brain extracellular space. *J. Biol. Chem.* **287,** 43108–43115
53. Sharples, R. A., Vella, L. J., Nisbet, R. M., Naylor, R., Perez, K., Barnham, K. J., Masters, C. L., and Hill, A. F. (2008) Inhibition of γ-secretase causes increased secretion of amyloid precursor protein C-terminal fragments in association with exosomes. *FASEB J.* **22,** 1469–1478
54. Vilette, D., Laulagnier, K., Huor, A., Alais, S., Simoes, S., Maryse, R., Provansal, M., Lehmann, S., Andreoletti, O., Schaeffer, L., Raposo, G., and Leblanc, P. (2015) Efficient inhibition of infectious prions multiplication and release by targeting the exosomal pathway. *Cell. Mol. Life Sci.* **72,** 4409–4427
55. Burgos, P. V., Mardones, G. A., Rojas, A. L., daSilva, L. L., Prabhu, Y., Hurley, J. H., and Bonifacino, J. S. (2010) Sorting of the Alzheimer's disease amyloid precursor protein mediated by the AP-4 complex. *Dev. Cell* **18,** 425–436
56. De Strooper, B., Iwatsubo, T., and Wolfe, M. S. (2012) Presenilins and γ-secretase: structure, function, and role in Alzheimer disease. *Cold Spring Harb. Perspect. Med.* **2,** a006304
57. Wolfe, M. S. (2013) Toward the structure of presenilin/γ-secretase and presenilin homologs. *Biochim. Biophys. Acta* **1828,** 2886–2897
58. Chan, R. B., Oliveira, T. G., Cortes, E. P., Honig, L. S., Duff, K. E., Small, S. A., Wenk, M. R., Shui, G., and Di Paolo, G. (2012) Comparative lipidomic analysis of mouse and human brain with Alzheimer disease. *J. Biol. Chem.* **287,** 2678–2688
59. Urwin, H., Ghazi-Noori, S., Collinge, J., and Isaacs, A. (2009) The role of CHMP2B in frontotemporal dementia. *Biochem. Soc. Trans.* **37,** 208–212
60. Massey, L. K., Mah, A. L., Ford, D. L., Miller, J., Liang, J., Doong, H., and Monteiro, M. J. (2004) Overexpression of ubiquilin decreases ubiquitination and degradation of presenilin proteins. *J. Alzheimers Dis.* **6,** 79–92
61. Ford, D. L., and Monteiro, M. J. (2007) Studies of the role of ubiquitination in the interaction of ubiquilin with the loop and carboxyl terminal regions of presenilin-2. *Biochemistry* **46,** 8827–8837
62. Kang, E. L., Biscaro, B., Piazza, F., and Tesco, G. (2012) BACE1 endocytosis and trafficking are differentially regulated by ubiquitination at lysine 501 and the di-leucine motif in the C terminus. *J. Biol. Chem.* **287,** 42867–42880
63. Yeates, E. F., and Tesco, G. (2016) The endosomal-associated deubiquitinating enzyme USP8 regulates BACE1 ubiquitination and degradation. *J. Biol. Chem.* **291,** 15753–15766
64. Lee, J.-G., Takahama, S., Zhang, G., Tomarev, S. I., and Ye, Y. (2016) Unconventional secretion of misfolded proteins promotes adaptation to proteasome dysfunction in mammalian cells. *Nat. Cell Biol.* **18,** 765–776
65. Azevedo, C., and Saiardi, A. (2016) Why always lysine? The ongoing tale of one of the most modified amino acids. *Adv. Biol. Regul.* **60,** 144–150
66. Chivet, M., Hemming, F., Pernet-Gallay, K., Fraboulet, S., and Sadoul, R. (2012) Emerging role of neuronal exosomes in the central nervous system. *Front. Physiol.* **3,** 145
67. Rajendran, L., Honsho, M., Zahn, T. R., Keller, P., Geiger, K. D., Verkade, P., and Simons, K. (2006) Alzheimer's disease β-amyloid peptides are released in association with exosomes. *Proc. Natl. Acad. Sci.* **103,** 11172–11177
68. Rajendran, L., Knobloch, M., Geiger, K. D., Dienel, S., Nitsch, R., Simons, K., and Konietzko, U. (2007) Increased Aβ production leads to intracellular accumulation of Aβ in flotillin-1-positive endosomes. *Neurodegener. Dis.* **4,** 164–170
69. Yuyama, K., Sun, H., Usuki, S., Sakai, S., Hanamatsu, H., Mioka, T., Kimura, N., Okada, M., Tahara, H., Furukawa, J., Fujitani, N., Shinohara, Y., and Igarashi, Y. (2015) A potential function for neuronal exosomes: sequestering intracerebral amyloid-β peptide. *FEBS Lett.* **589,** 84–88
70. Meckler, X., and Checler, F. (2016) Presenilin 1 and presenilin 2 target γ-secretase complexes to distinct cellular compartments. *J. Biol. Chem.* **291,** 12821–12837
71. Yonemura, Y., Futai, E., Yagishita, S., Kaether, C., and Ishiura, S. (2016) Specific combinations of presenilins and Aph1s affect the substrate specificity and activity of γ-secretase. *Biochem. Biophys. Res. Commun.* **478,** 1751–1757
72. Acx, H., Chávez-Gutiérrez, L., Serneels, L., Lismont, S., Benurwar, M., Elad, N., and De Strooper, B. (2014) Signature Aβ profiles are produced by different γ-secretase complexes. *J. Biol. Chem.* **289,** 4346–4355
73. Fernandez, M. A., Klutkowski, J. A., Freret, T., and Wolfe, M. S. (2014) Alzheimer presenilin-1 mutations dramatically reduce trimming of long amyloid β-peptides (Aβ) by γ-secretase to increase 42-to-40-residue Aβ. *J. Biol. Chem.* **289,** 31043–31052
74. Yan, Y., and Wang, C. (2007) Aβ40 protects non-toxic Aβ42 monomer from aggregation. *J. Mol. Biol.* **369,** 909–916
75. Pauwels, K., Williams, T. L., Morris, K. L., Jonckheere, W., Vandersteen, A., Kelly, G., Schymkowitz, J., Rousseau, F., Pastore, A., Serpell, L. C., and Broersen, K. (2012) Structural basis for increased toxicity of pathological Aβ42:Aβ40 ratios in Alzheimer disease. *J. Biol. Chem.* **287,** 5650–5660
76. Murray, M. M., Bernstein, S. L., Nyugen, V., Condron, M. M., Teplow, D. B., and Bowers, M. T. (2009) Amyloid β-protein: Aβ40 inhibits Aβ42 oligomerization. *J. Am. Chem. Soc.* **131,** 6316–6317
77. McGowan, E., Pickford, F., Kim, J., Onstead, L., Eriksen, J., Yu, C., Skipper, L., Murphy, M. P., Beard, J., Das, P., Jansen, K., DeLucia, M., Lin, W.-L., Dolios, G., Wang, R., *et al.* (2005) Aβ42 is essential for parenchymal and vascular amyloid deposition in mice. *Neuron* **47,** 191–199
78. Xu, F., Fu, Z., Dass, S., Kotarba, A. E., Davis, J., Smith, S. O., and Van Nostrand, W. E. (2016) Cerebral vascular amyloid seeds drive amyloid β-protein fibril assembly with a distinct anti-parallel structure. *Nat. Commun.* **7,** 13527
79. De Strooper, B., and Chávez Gutiérrez, L. (2015) Learning by failing: ideas and concepts to tackle γ-secretases in Alzheimer disease and beyond. *Annu. Rev. Pharmacol. Toxicol.* **55,** 419–437
80. Golde, T. E., Koo, E. H., Felsenstein, K. M., Osborne, B. A., and Miele, L. (2013) γ-Secretase inhibitors and modulators. *Biochim. Biophys. Acta* **1828,** 2898–2907
81. Sevigny, J., Chiao, P., Bussière, T., Weinreb, P. H., Williams, L., Maier, M., Dunstan, R., Salloway, S., Chen, T., Ling, Y., O'Gorman, J., Qian, F., Arastu, M., Li, M., Chollate, S., *et al.* (2016) The antibody aducanumab reduces Aβ plaques in Alzheimer's disease. *Nature* **537,** 50–56
82. Bohdanowicz, M., Balkin, D. M., De Camilli, P., and Grinstein, S. (2012) Recruitment of OCRL and Inpp5B to phagosomes by Rab5 and APPL1 depletes phosphoinositides and attenuates Akt signaling. *Mol. Biol. Cell* **23,** 176–187

Disruption of amyloid precursor protein ubiquitination selectively increases amyloid β (Aβ) 40 levels via presenilin 2-mediated cleavage

Rebecca L. Williamson, Karine Laulagnier, André M. Miranda, Marty A. Fernandez, Michael S. Wolfe, Rémy Sadoul and Gilbert Di Paolo

J. Biol. Chem. 2017, 292:19873-19889.
doi: 10.1074/jbc.M117.818138 originally published online October 11, 2017
